Compilation and Forecasting of Paleoliquefaction Evidence for the Strength of Ground Motions in the U.S. Pacific Northwest

Ryan A. Rasanen[1], Nasser A. Marafi[2], and Brett W. Maurer[1]

Abstract: In the U.S. Pacific Northwest (PNW), the historic earthquake record is often insufficient to provide inputs to seismic-hazard analyses or to inform ground-motion predictions for certain seismic sources (e.g., the Cascadia Subduction Zone, CSZ). As a result, paleoseismic studies are commonly used to infer information about the seismic hazard. However, among the many forms of coseismic evidence, soil liquefaction provides the best, if not only, evidence from which the intensities of previous ground motions may be constrained. Accordingly, the overarching goal of this research is to use paleoliquefaction to elucidate previous ground motions in the PNW – both for CSZ events and others – and to further constrain the locations, magnitudes, and recurrence rates of such ruptures. Towards that goal, this paper: (i) reviews current paleoliquefaction inverse-analysis methods and their limited, prior applications in the PNW; (ii) compiles all PNW paleoliquefaction evidence from the literature into a GIS database, resulting in data from 185 study sites (e.g., feature locations, types, sizes, and ages); and (iii) develops maps – specific to the CSZ – that forecast paleoliquefaction for 30 different simulations of a CSZ event. These maps can be used to guide field explorations for new evidence, such that they are conducted efficiently and strategically, considering the apparent utility of evidence toward constraint of CSZ ground-motion models. Of additional utility, this process provides regional ground-motion predictions for physics-based simulations of an M9 event, to include expected site effects. Collectively, the maps of expected shaking intensity and liquefaction may be useful in downstream hazard modelling, regional loss estimation, policy development, and science communication. Ultimately, as more paleoliquefaction evidence is identified and studied, better constraint of regional ground-motion hazards will result.

1. Introduction

1.1 Significance of Paleoliquefaction Evidence

In regions experiencing infrequent moderate-to-large earthquakes, the historic record may be insufficient to provide accurate inputs to seismic-hazard analyses (i.e., the locations, magnitudes, and recurrence-rates of fault ruptures) or to inform ground-motion predictions for certain seismic sources. As an example, the 1700 A.D. Cascadia Subduction Zone (CSZ) earthquake was likely far bigger than

[1] Department of Civil and Environmental Engineering, University of Washington, Seattle USA.
[2] Risk Management Solutions, Newark, California USA.

any subsequent rupture in the U.S. Pacific Northwest (PNW), yet there is little-to-no eyewitness account of it (Thrush and Ludwin 2007), let alone ground-motion records. As a result, paleoseismic evidence must be relied on to elucidate the seismic hazard. In the case of the CSZ, the 1700 earthquake is believed to be one of approximately 40 similar events during the past 10,000 years, all judged to be M8.0 to M9.0 or greater, as inferred from dendrochronology (e.g., Atwater et al., 1991), turbidites (e.g., Goldfinger et al., 2012; Atwater et al., 2014), tsunami deposits (e.g., Peters et al., 2007), soil liquefaction (e.g., Obermeier 1995), microfossils (e.g., Engelhart et al., 2013), geochemical markers (e.g., O'Donnell et al., 2017), and seafloor morphology (e.g., Watt et al., 2017), among other indicators of seismicity. Collectively, this evidence has been used to infer a length of fault rupture, which leads to an estimate of earthquake magnitude (e.g., Petersen et al., 2014).

Given the premise of a full-fault M9 CSZ earthquake, various ground-motion predictions have been made (e.g., USGS, 2017). These include – most recently – a suite of broadband synthetic seismograms (i.e., ground-motion time histories) (Frankel et al., 2018a; Wirth et al., 2018) that predict motions on a 1-km grid across the PNW. This suite includes 30 different realizations to reflect the uncertainty of key parameters (e.g., the down-dip limit of fault rupture; the slip distribution and location of asperities; and hypocenter location). Given that the last CSZ event occurred in 1700, these parameters are unknown for all such events. Shown in Fig. 1 are two such realizations. While both simulate a full-fault M9 CSZ rupture, it can be seen that predicted ground-motions vary significantly in some locales (e.g., peak ground velocities may vary by 400%). By corollary, the expected impacts on the built and living environments would also be very different (Marafi et al., 2019, 2020).

Notably, the actual ground motions experienced in 1700 (and in other paleo events) can be determined only through inverse analysis of coseismic evidence. But, among the many paleoseismic artifacts that have been documented, only soil liquefaction and landslides are presently capable of "recording" the intensity of ground motions. As summarized in Table 1, the date of an earthquake, and therefore recurrence-rate, can be derived from many types of evidence (although some are more likely to illuminate older records, owing to preservation potential or ease of discovery). Considering the spatial extent of such evidence (e.g., the length of coastline affected), an earthquake's location and magnitude may be estimated, at least crudely. However, most artifacts are only loosely correlated to the intensity of shaking, if at all. That is, the evidence may suggest that earthquake occurred, but do little or nothing to quantify the ground motions experienced. In this regard, soil liquefaction and landslides are more than just proxies of shaking, given that they could be used to quantitatively constrain its intensity across an affected region. This distinction arises because mechanistic models exist for predicting these phenomena as a function of ground-motion intensity measures (IMs).

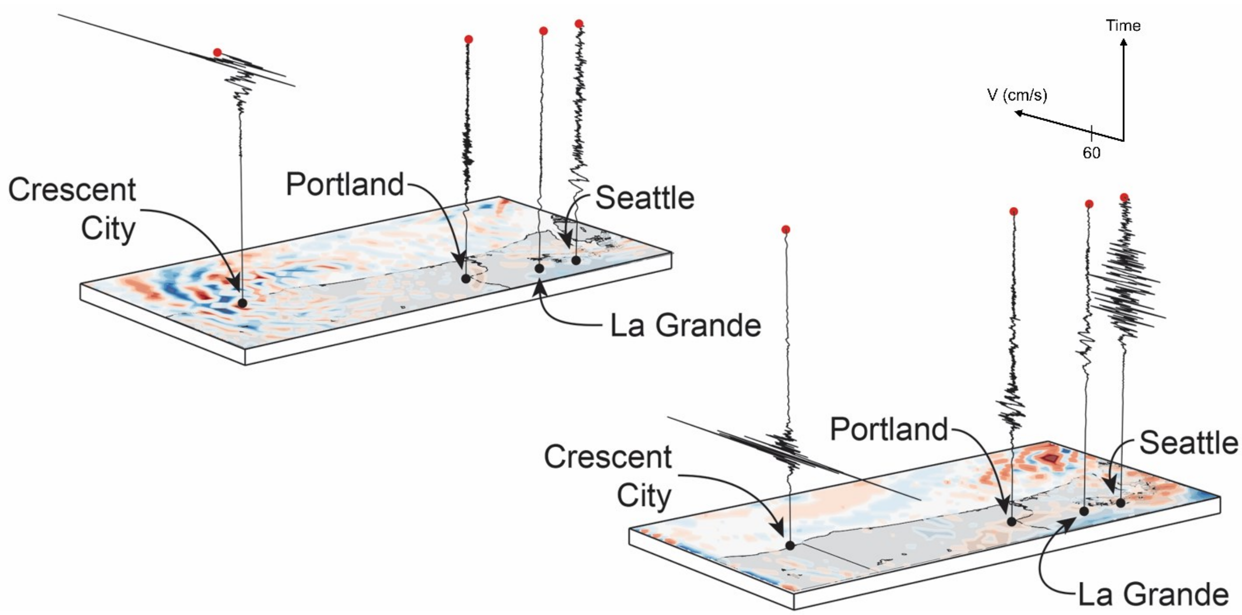

Fig. 1. Two ground-motion predictions of a M9 CSZ earthquake, reflecting the influence of salient modeling uncertainties (traces are ground velocity for the duration of the event; colors show a snapshot of seismic waves at a moment in time). The sensitivity of predictions to modeling uncertainties is readily apparent via the large discrepancies at some locales (e.g., in Seattle). Simulations by Frankel et al. (2018a) and Wirth et al. (2018).

Table 1. Synopsis of evidence from which paleoseismic parameters may be derived.

Paleoseismic Evidence	**Earthquake Parameters Obtainable from Evidence**		
	Rupture Date / Recurrence Rate	Rupture Location and Magnitude	Resultant Ground Motions
Dendrochronology	✓	✓	✕
Diatoms / Microfossils	✓	✓	✕
Other Subsidence Markers	✓	✓	✕
Tsunami Deposits / Impacts	✓	✓	✕
On- & Off-Shore Turbidite Records	✓	✓	✕
On-Fault Evidence	✓	✓	✕
Landslides / Rockfall	✓	✓	✓
Soil Liquefaction	✓	✓	✓

In conventional hazard analyses, wherein the seismic loading is given, these models are widely used to predict future outcomes (e.g., liquefaction). In paleoseismic studies, wherein the outcome is given (e.g., liquefaction did or did not occur), the models can be inverted to back-calculate the ground motions that likely would, and would not, produce the observation. It should be noted, however, that while paleoliquefaction features have been identified at over 180 locations in the PNW, including many that formed ca. 1700, paleolandslides with constrained ages are less common. As an example, landslides have yet to be linked to any CSZ earthquake (Struble et al. 2017). In addition, aseismic landslides occur frequently and are difficult to distinguish from their seismic counterparts, whereas aseismic ground failures resembling liquefaction are less common (e.g., Obermeier et al. 2011). Thus, liquefaction presently provides the best, and perhaps only, evidence from which the intensity of shaking in PNW paleoearthquakes may be quantified. This includes ruptures in the CSZ, but also on crustal faults in the Puget-Willamette Lowlands (e.g., the Seattle and Whidbey Island Faults) which have similarly not ruptured in modern history. The potential value of paleoliquefaction evidence has previously been proven in many other seismic zones (e.g., Tuttle and Hartleb, 2012; Bastin et al., 2016).

1.2 Motivation and Objectives

The long-term goal of this research is to use paleoliquefaction data to determine the strength of past ground motions in the PNW – both for CSZ events and others – and to further elucidate the locations, magnitudes, and recurrence rates of such ruptures. Towards that end, compilation of *regional* evidence is needed to answer questions of greatest interest (e.g., "When, on which fault, and of what magnitude was a paleoearthquake?" or "Which CSZ ground-motion simulations are plausible realizations of those experienced in 1700?"). This will be shown subsequently though a review of paleoliquefaction analytics. While analysis of an individual site could render ground motion IM values that likely would, or would not, produce an observation at that site, there will inevitably be an infinite number of these respective values. As an example, the minimum peak ground acceleration (*PGA*) requisite for liquefaction in a highly susceptible soil is ~ 0.1 g (de Magistris et al., 2013). If paleoliquefaction is observed at such a site, the *PGA* was therefore likely at least 0.1 g, but is otherwise unknown. A similarly loose upper-bound constraint is obtainable from a site where no paleliquefaction is observed, if the subsurface has very low susceptibility. Moreover, most *PGA* values could result from a small, nearby rupture, or from a large, distant rupture. The elucidation of regional ground-motion IM patterns thus requires spatially distributed study sites having a range of liquefaction susceptibilities, with and without observed manifestations of liquefaction. However, while many individual study sites have been documented in the PNW, these data exist across numerous publications and have not been compiled. Such an effort was undertaken nearly a decade ago in the Central-Eastern United States, where paleoliquefaction evidence was aggregated by Tuttle and Hartleb (2012), the results of which were used to inform seismic hazard analyses for nuclear facilities (NRC, 2012). The PNW has similarly ambiguous seismic records but lacks an analogous resource. As a result, regional scale paleoliquefaction studies have not been performed, and thus, the available field evidence has arguably not been exploited. Accordingly, the first objective of this paper is to compile existing paleoliquefaction evidence from the PNW into a community GIS database.

It is also critical that additional evidence be discovered, compiled, and analyzed, since better constraint of regional ground-motions in past earthquakes will result. However, a field search of the entire region would be extremely cost-prohibitive. Moreover, and using the CSZ as an example, there are infinite locales where the confirmed presence or absence of 1700 liquefaction would do little to inform or constrain ground-motion predictions (e.g., because various predictions lead to similar expectations of liquefaction). For field pursuits to be conducted more efficiently and strategically, it would be helpful to identify locations where uncertainties in ground-motion simulations (e.g., Frankel et al. 2018a; Wirth et al. 2018) give rise to significant differences in liquefaction predictions. Thus, the second objective of this paper is to develop maps – specific to the CSZ – that identify and prioritize where paleoliquefaction evidence should be searched for. This will be achieved, in part, using 30 different physics-based ground motions simulations of an M9 CSZ earthquake.

In the following, a summary of paleoliquefaction analytics is first presented. It will highlight: (i) the need to study evidence regionally; and (ii) prior applications of these analytics in the PNW, which while limited, hint at the potential for paleoliquefaction to provide new insights into persistent uncertainties. Next, the contents of the compiled paleoliquefaction database are described, and lastly, maps that guide future field expeditions for evidence in the CSZ are developed and discussed.

2. Summary of Paleoliquefaction Analysis Methods and Their Application in the PNW

While paleoliquefaction has been widely documented in the PNW, there are few studies in which seismic data has been derived from it (other than event age). Two of these studies are noted in the ensuing summary, to include emphasis of their shortcomings. It should be stressed, however, that these shortcomings are those of the tools then-available, which will serve to highlight recent advances. If not for these and other seminal studies, the database compiled herein would not be possible.

The study of paleoliquefaction has three phases: (i) field identification and interpretation; (ii) dating; and (iii) constraint of the earthquake magnitude and/or ground motion under which it formed. The reader is referred to the overviews of field interpretation by Obermeier et al. (2001; 2005), and to the field investigations of Obermeier and Dickenson (2000), Tuttle (2001), Talwani and Schaeffer (2001), Cox et al. (2007), and Tuttle et al. (2002a; 2002b; 2005), among others, for specific case studies. In addition, Sims and Garvin (1995), Quigley et al. (2013), Bastin et al. (2016), and Maurer et al. (2019) discuss field interpretation specific to spatiotemporally clustered earthquakes. Once identified, features may be dated via radiocarbon, optically stimulated luminescence, archeological or stratigraphic context, and soil development indicators, such as weathering and biologic activity. A comprehensive overview of paleoliquefaction dating methods is provided by Tuttle and Hartleb (2012). The techniques by which earthquake magnitude and/or shaking intensity are quantitatively constrained are generally called back- or inverse-analysis methods. The two most common to-date are the "magnitude-bound" method (e.g., Ambraseyes, 1988; Olson et al., 2005a; Maurer et al., 2015a) and the "site-specific geotechnical analysis," or for brevity, the "site-specific" method (e.g., Olson et al., 2005b; Rodriguez-Marek and Ciani, 2008; Green et al., 2005, 2014).

2.2 Magnitude-Bound Method

The magnitude-bound method uses a correlation relating earthquake magnitude to the site-to-source distance of the most distal site of liquefaction. Developed from observations in modern earthquakes, these correlations traditionally use data from variable geologic-tectonic settings and provide a lower-bound estimate of magnitude. As an example, Fig. 2 presents ten correlations from the literature.

One of these correlations was used by Bourgeois and Johnson (2001), who documented at least three episodes of paleoliquefaction in Washington's Snohomish River delta, with one episode dated ca. 910-990, coinciding with possible events on the Seattle Fault and CSZ. Bourgeois and Johnson (2001) deduced that: (1) a Seattle Fault rupture ≥ M_w7 would generate liquefaction 50 km away at the study site; and (2) other faults in the southern Puget Lowland, 75-120 km away, would require earthquakes ≥ M_w 6.5-7 to do so. Importantly, the maximum site-to-source distance of liquefaction is a function of numerous region- and site-specific factors. These include seismic source traits (e.g., focal depth and mechanism), transmission characteristics (e.g., ground motion attenuation and site effects), liquefaction susceptibility (e.g., density, fines-content, plasticity, and saturation); and subsurface stratigraphy (e.g., the quantity, depth, and thickness of all liquefiable strata, and the properties of overlying non-liquefiable strata), none which is directly accounted for by empirical magnitude-bound curves. Because these factors all vary (as reflected by the range of correlations in Fig. 2), region-specific correlations can provide more accurate estimates than those developed from global data (Olson et al., 2005a, 2005b; Maurer et al., 2015a). Shortcomings aside, the magnitude-bound method inherently requires compilation of regional evidence, since the liquefaction field resulting from an event must be fully delineated to properly ascribe a minimum rupture magnitude.

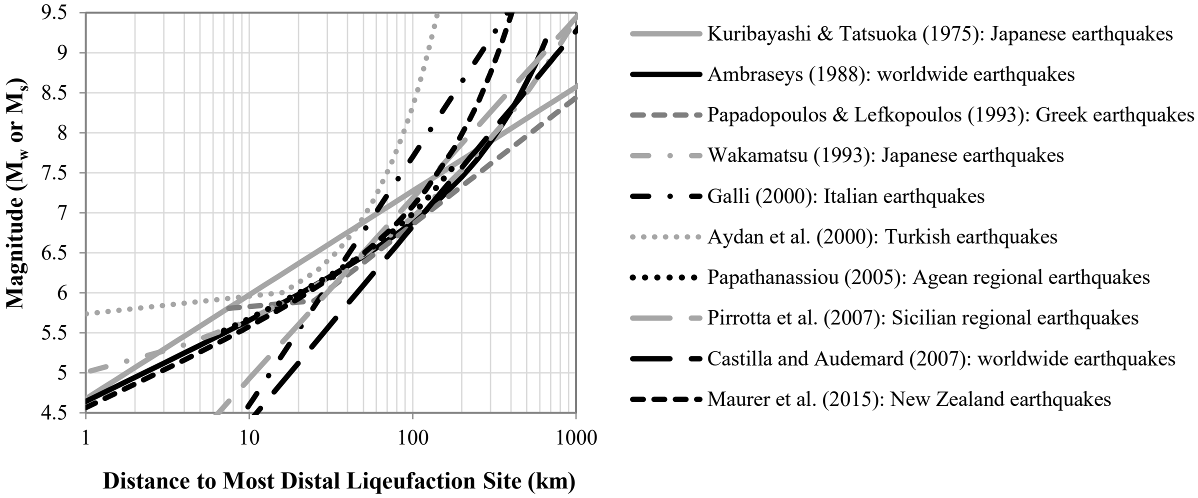

Fig. 2. Magnitude-bound curves for various geographic and tectonic settings, where site-to-source distance is quantified in terms of epicentral distance.

2.2 Site-Specific Geotechnical Analysis

The second, more technical site-specific method uses models based on in-situ geotechnical tests. In forward hazard analyses, wherein the seismic loading is given, these models predict the future triggering and manifestation of liquefaction (e.g., Green et al., 2019; Geyin and Maurer, 2020). In paleoliquefaction studies, wherein the outcome is given, the models are "inverted" to derive information about the causative earthquake. While implementations of the site-specific method have varied with time and place (e.g., Martin and Clough, 1990; Hayati and Andrus, 2008; Hu et al., 2002; Holzer et al., 2015; Gheibi et al., 2020; Rasanen and Maurer, 2021), variants can collectively: (i) identify combinations of rupture magnitude and ground-motion intensity likely to produce outcomes at individual sites (most applicable while the number of study sites is limited); (ii) probabilistically geolocate a seismic source from an evidence field and determine its magnitude (most applicable where faults are blind, or where prospective causative faults are plentiful); or (iii) compute the likelihood that a simulated ground-motion is a plausible realization of that experienced prior, as evidenced by the presence or absence of liquefaction (most applicable when competing forecasts are available).

With respect to the latter, and using the CSZ as an example, the likelihood that a ground-motion simulation represents a past event, given a set of field observations, may be computed as the product of the probabilities of those observations, conditioned on the simulation. Thus, the likelihood that a rupture had certain traits (e.g., location (L), geometry (G), and magnitude $(M_w)\ldots$) given a set (x) of field observations at *N* different sites, can be computed as:

$$Likelihood\,(L, G, M_w \ldots | x) = P(X = x | L, G, M_w \ldots) = \prod_{i=1}^{N} P(X_i = x_i | L, G, M_w \ldots) \quad (1)$$

Where $P(X_i = x_i | L, G, M_w \ldots)$ is the probability of the observation at site *i* (liquefaction or no liquefaction) given an earthquake with parameters *L*, *G*, M_w, etc. By repeating for numerous simulations, the most plausible realizations of a past event can be probabilistically identified via the likelihood function (product of the probabilities of *N* observations), such that different combinations of *L*, *G*, M_w, etc. will be found more and less likely to produce the observed field evidence. Like the magnitude-bound approach, this method inherently relies on compilation of regionally distributed study sites. In Eq. (1), the probability of a field observation is computed as $P(\text{Liquefaction}|PGA, M_w)$ if manifestations of liquefaction are observed, and as 1 - $P(\text{Liquefaction}|PGA, M_w)$ otherwise. $P(\text{Liquefaction}|PGA, M_w)$ is the probability of observing liquefaction at a site, given ground-motion parameters *PGA* and M_w, as computed by a model of liquefaction triggering or, more ideally, liquefaction surface manifestation (embedded in which is a triggering model). As an example, Geyin and Maurer (2020) proposed fragility functions conditioned on three different liquefaction manifestation models (e.g., the liquefaction potential index, *LPI*, proposed by Iwasaki et al., 1978) computed using six different liquefaction triggering models (e.g., Green et al., 2019) such that users can select from, or average, 18 total functions. The results of such an analysis could in-turn inform CSZ modeling uncertainties such as: What were the extents of fault rupture? Where was the hypocenter? What was the direction of rupture propagation? Where were the rupture asperities?

The authors are aware of one prior application of the "site-specific" method in the PNW. Obermeier and Dickenson (2000) conducted field searches on six Columbia River islands, building upon and benefiting from many previous efforts (e.g., as compiled by Atwater, 1994). This resulted in the documented presence, or judged absence, of paleoliquefaction on each island, with features generally constrained to the year 1700 and decreasing in size and frequency moving inland. Obermeier and Dickenson (2000) used liquefaction models to back-calculate the *PGA*s that occurred on this transect in 1700. Notably, they suggest that *PGA*s were as low as 20% of those predicted by recent M9 simulations (Frankel et al., 2018a; Wirth et al., 2018). As stated by Obermeier and Dickenson (2000): "Our interpreted levels of shaking are considerably lower than current estimates that use theoretical and statistical models to predict ground motions of subduction earthquakes in the Cascadia region."

While these findings are provocative, they come with an important series of caveats. *First*, Obermeier and Dickenson (2000) utilized the liquefaction triggering model of Youd and Nobel (1997), to which standard penetration test (SPT) data from a site is input. However, the Youd and Nobel (1997) model is not used today - a sequence of major modifications and additions have since been made (e.g., to account for factors then unknown to be significant). *Second*, as new in-situ test methods have been developed, SPT-based liquefaction triggering models have fallen out of favor, with the cone penetration test (CPT) now recognized as the ideal (NRC, 2016). *Third*, because the study sites were located on islands, SPT equipment was not actually deployed. In its place, a hand-held variant was used (referred to today as a dynamic cone penetration test) and then correlated to SPT measurements by unknown means. The results of this test were then input to the Youd and Nobel (1997) model, which predicts liquefaction triggering at depth within a soil profile. *Fourth*, to predict whether liquefaction that triggered at depth should be expected to manifest at the surface, Obermeier and Dickenson (2000) utilized the Ishihara (1985) "H1-H2" chart (which predicts the thickness of a surficial crust needed to suppress surface manifestation). However, when tested on more recent earthquakes, this method has in some events exhibited prediction efficiencies similar to random guessing (van Ballegooy et al. 2015). Newer manifestation models informed by significantly larger datasets (e.g., van Ballegooy et al. 2014; Maurer et al. 2015b) are now available. *Fifth*, none of the methods adopted by Obermeier and Dickenson (2000) accounted for uncertainty (e.g., probabilistic liquefaction models were not available at the time). Notably, deterministic liquefaction models like Youd and Nobel (1997) traditionally have embedded conservatism, such that the binomial threshold for triggering corresponds to a relatively low probability of liquefaction (e.g., 15%). The *PGA*s constrained by Obermeier and Dickenson (2000) may thus correspond to the 15th percentile of what possibly occurred, rather than to a best estimate.

As stated by Obermeier and Dickenson (2000): "Our arguments are based largely on qualitative inferences of liquefaction susceptibility supported by preliminary geotechnical data." The true 1700 ground-motions thus remain enigmatic. Considering major advances in liquefaction analytics made over the last 20 years, CSZ paleoliquefaction features can and should be investigated using modern tools and methods. As concluded by Obermeier and Dickenson (2000): "More paleoliquefaction and geotechnical field studies are needed to bracket the strength of shaking."

3. Compilation of PNW Paleoliquefaction Evidence

Paleoliquefaction evidence in the PNW was compiled from 24 publications, as summarized in Table 2. The information compiled from each reference includes (when available): study site locations and feature morphologies (e.g., sand-blow thickness and dike width); dating information; important comments from the author; and citations to all original source documents, data, and figures.

Table 2. Literature reviewed and compiled in the paleoliquefaction database.

Reference	Study Region(s)	Reference ID
Atwater (1992)	Washington coast	1
Atwater (1994)	Columbia River	2
Atwater (2020)	Puget Sound (West Point), Washington	3
Bourgeois and Johnson (2001)	Puget Sound (Snohomish River delta), Washington	4
Briggs (1994)	Oregon coast	5
Clague et al. (1992)	Fraser River delta, British Columbia	6
Clague et al. (1997)	Fraser River delta (Annacis Island), British Columbia	7
Davis (2019)	Puget Sound (Duwamish River), Washington	8
Fiedorowicz (1997)	Oregon coast	9
Kelsey et al. (2002)	Oregon coast	10
Martin and Bourgeois (2012)	Hood Canal (Skokomish River delta and Lynch Cove), Washington; Lake Sammamish (Issaquah Creek), Washington	11
Obermeier (1995)	Chehalis River, Washington; Columbia River	12
Peterson and Madin (1997)	Columbia River; Washington coast; Oregon coast	13
Peterson et al. (2005)	Oregon coast	14
Peterson et al. (2008)	Oregon coast	15
Peterson et al. (2013)	Washington coast	16
Peterson et al. (2014)	Willamette River, Oregon; Oregon coast; Washington coast	17
Polenz et al. (2010)	Hood Canal (Skokomish Valley), Washington	18
Sherrod (2001)	Puget Sound, Washington	19
Sherrod et al. (2004)	Puget Sound, Washington	20
Sims (2002)	Calapooia River, Oregon	21
Takada and Atwater (2004)	Columbia River	22
Whistler et al. (2002)	Lake Sammamish (Issaquah Creek), Washington	23
Zehfuss (2005)	Puget Sound, Washington	24

Tuttle and Hartleb (2012), under the auspices of the Nuclear Regulatory Commission (NRC, 2012), previously developed an analogous GIS database for the Central and Eastern United States, compiling data for subsequent distribution to the research community. This seminal resource, which included multiple seismic zones but did not extend west of the Mississippi River, serves as an excellent guide for aggregating paleoliquefaction data elsewhere. To facilitate continuity between regions, the data fields proposed by Tuttle and Hartleb (2012) were adopted with minor additions for the PNW. These additions include fields to describe the thickness and lithology of the non-liquefiable capping layer, or "crust", as well as dendrochronological information, which field geologists have compiled at some sites in the PNW. A complete listing of the data-field names is given in Table 3, as are detailed descriptions of each attribute. Figure 3 illustrates several of these attributes, including: sand-blow thickness, width, and length; dike width; and sill thickness.

Table 3. Paleoliquefaction database field names and their descriptions.

Field Name	Description
SITE_NAME	Alphabetic designator of study area.
FEAT_ID	Unique alphabetic identifier for paleoliquefaction features within the same study area (e.g., Columbia River-01 and Columbia River-02). If a letter is present after the number, then there are multiple liquefaction events in the geologic record at the same location (e.g., Columbia River-06a and Columbia River-06b).
XCOORD	Numeric value of longitude, in decimal degrees.
YCOORD	Numeric value of latitude, in decimal degrees.
COORD_ORIG	Alphabetic description of reference from which study site coordinates are derived from. Some locations were digitized from maps, rather than obtained directly from coordinates. Site coordinates, as given in reports, may also have uncertainty due to limited measurement precision. For example, several Peterson and Madin (1997) study sites were in water (likely from GPS measurement error). In some cases, obvious errors were corrected by the authors (e.g., moving the coordinates to a riverbank near the original coordinates). In other cases, coordinates in water were left as-is.
OBS_TYPE	Alphabetic description of where/how paleoliquefaction was discovered (e.g., river cut bank, trench, borehole, geoslice).
FEAT_TYPE	Alphabetic description of feature type observed (e.g., sand blow, dike, sill, soft sediment deformation).
SSD_DESCR	Alphabetic description of seismic related soft sediment deformation (SSD) features (e.g., convolute beds, flame structure).
FEAT_REF	Alphabetic description of reference where paleoliquefaction feature information was obtained.
SB_THICK SB_WIDTH SB_LENGTH DK_WIDTH SILL_THICK	Numeric values of dimensions of sand blow thickness, sand blow width, sand blow length, dike width, and sill thickness, respectively. All dimensions are in cm and given as maximums. Of course, features may not be fully uncovered or delineated in the field, so maximum dimensions may be larger. Dimensions are either directly supplied by original authors or were inferred from to-scale figures. When available, sand blow thickness is measured adjacent to the vent. Sand blows are assumed circular, such that cross-sectional measurements of their size are assumed representative. The value "present" was assigned to sites where sand blows, dikes, or sills were documented but not measured.
CAP_THICK	Numeric value for the thickness of the capping layer, if provided.
CAP_LITH	Alphabetic description of type of soil the capping layer is mainly composed of, if provided.
DIM_REF	Alphabetic description of reference which provides paleoliquefaction feature dimensions either specifically in writing, from tables, or from to-scale figures.
MAX_CAL_2S	Alphanumeric description of two standard deviation maximum calibrated age range specified as cal AD or cal BC.
MIN_CAL_2S	Alphanumeric description of two standard deviation minimum calibrated age range specified as cal AD or cal BC.
MAX_CAL	Numeric maximum calibrated age in years AD (negative values indicate years BC). The single value given for maximum calibrated age is the two standard deviation limit. For example, if a site has a two standard deviation maximum calibrated age range of 1413-1642 AD, then the maximum calibrated age is 1413 AD.
MIN_CAL	Numeric minimum calibrated age in years AD (negative values indicate years BC). The single value given for minimum calibrated age is the two standard deviation limit. For example, if a site has a two standard deviation minimum calibrated age range of 1461-1878 AD, then the minimum calibrated age is 1878 AD.
C14_REF	Alphabetic description of reference which provides calibrated age or radiocarbon age. For sources which only provided radiocarbon ages, the Stuiver et al. (2020) CALIB program was used to convert radiocarbon ages to calibrated ages.
DENDRO_MAX	Alphanumeric maximum calibrated age in years AD from tree ring data.
DENDRO_MIN	Alphanumeric minimum calibrated age in years AD from tree ring data.
DENDRO_REF	Alphabetic description of reference which provides the dendrochronology data.
PREFAGEEST	Alphanumeric preferred age estimate in the format given by original authors. Some authors give an exact year, such as 1700 AD (Atwater, 1994), while others give qualitative descriptors, such as "slightly older than 130 BC" or "significantly younger than 1150 BC" (Obermeier, 1995). Preferred ages are based on radiocarbon, stratigraphy, archeology, or other dating methods. Additional details are provided in the COMMENT field where helpful.
PREFAGEREF	Alphabetic description of the source which provides the preferred age data.
STRAT	Alphabetic description of feature age based on stratigraphic relationships. For example, using the circa 1480 AD Mt St. Helen's ash layer to estimate a feature's age.
ARCHEO	Alphabetic description of feature age based on archaeological age data.
WEATHERING	Alphabetic description of degree of weathering of feature, or of surrounding sediments, to give an indication of the age of the feature or surrounding sediments.
COMMENT	Alphabetic description of salient comments/conclusions made by the original author(s), and other relevant information not captured in previous fields but extracted by the database compilers. There are three comment fields in total.

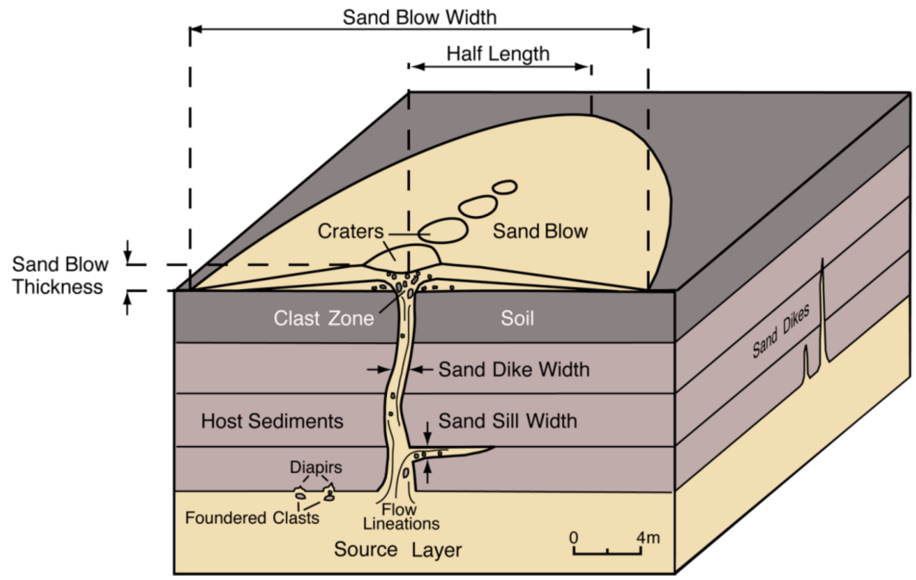

Fig. 3. Illustration of liquefaction-feature characteristics referenced in Table 3, including: sand-blow thickness, width, and length; dike width; and sill thickness. Figure from Tuttle and Hartleb (2012).

The resulting, curated dataset is available via the NHERI DesignSafe data depot at Rasanen et al. (2021) (https://doi.org/10.17603/ds2-fqkr-h615) and is provided as both a GIS map package and a flatfile spreadsheet. It should be noted, with respect to the attributes described in Table 3, that: (i) not all study sites contain information in all data fields (e.g., some lack dating information); (ii) many study sites have multiple liquefaction features, in which case features in a given locale are denoted by a single data point (e.g., Clague et al. (1992) documented 80 liquefaction features at a "site", but only provided a range of their sizes, in lieu of describing individual features); (iii) both radiocarbon dating methods of radiometric and accelerator mass dating are considered to give C14 dates; (iv) while all features in the database are judged to be of seismic origin based on conclusions made by the original investigators and reassessed by the current authors, the possibility of an aseismic cause nonetheless persists. In this regard, the criteria proposed by Obermeier (1996) for inferring seismic origin, further demonstrated by Obermeier et al. (2011), were used to provisionally rule out the possibility that features in the PNW were produced by aseismic geologic or climatic conditions.

In total, 185 study sites were compiled, as mapped in Fig. 4, and are respectively located in British Columbia (8), Oregon (43), and Washington (109). Additional sites reside along the banks, or on islands, of the Columbia River (25), which divides Oregon and Washington. Sites are otherwise concentrated in British Columbia's Fraser River delta, Oregon's Willamette River valley, Washington's Puget Sound, and in estuaries along the Pacific Coastline.

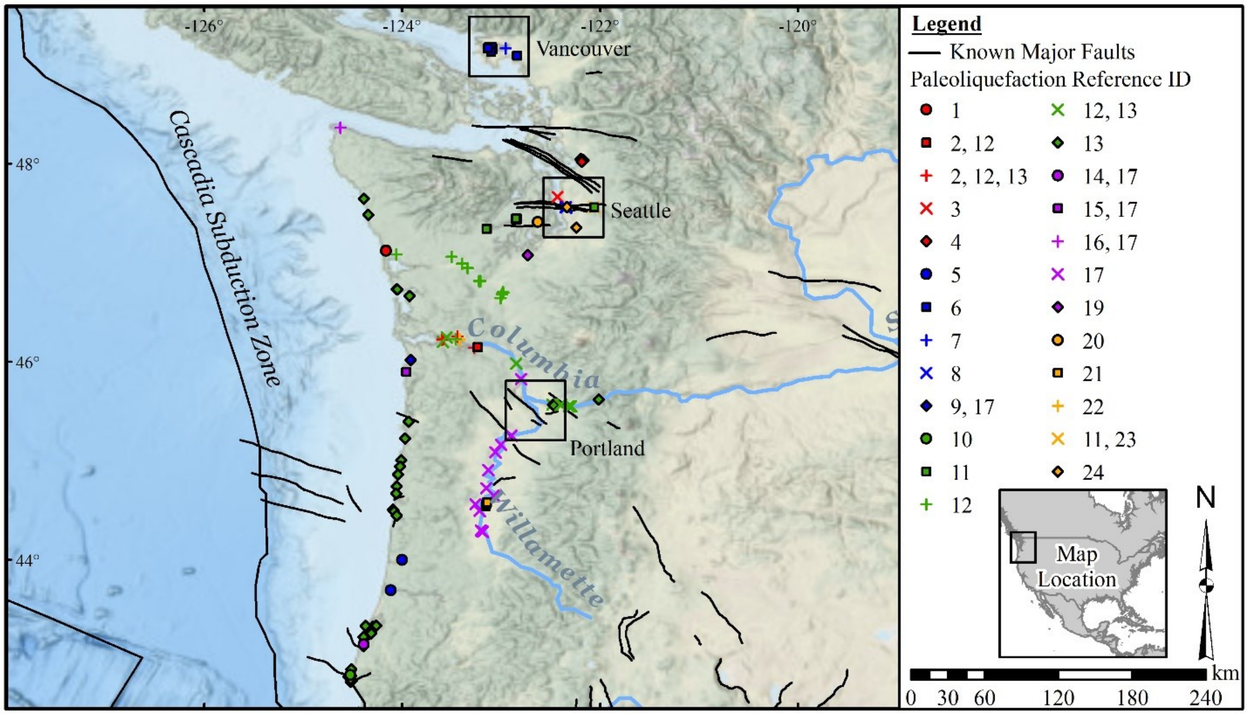

Fig. 4. Compilation of paleoliquefaction evidence. Reference IDs are given in Table 2.

The information compiled (see Table 3) allows for study sites to be symbolized by a variety of attributes (e.g., paleoliquefaction feature type, size, and age). Example products from the PNW database include the type of paleoliquefaction manifestation (e.g., sand blows or dikes) and the respective dimensions of the feature (e.g., sand blow thickness or dike width), as mapped in Fig. 5. In general, smaller, marginal features may more tightly constrain the intensity of past shaking, since this intensity was likely near the threshold for feature formation (i.e., for liquefaction triggering and manifestation). By corollary, larger features generally suggest prior loading far above such thresholds. However, because current liquefaction models predict the incidence of liquefaction manifestation more efficiently than the severity of manifestation (Maurer et al., 2015c), larger features may, at present, provide less quantitative constraint on the intensity of past shaking. The presence of large diameter features far from the coast (e.g., near the cities of Seattle and Vancouver) likely also indicates that not all features are associated with CSZ interface earthquakes, as will be further discussed. Additionally, as shown in Fig. 6, dating information – where available – can constrain the maximum calibrated age and/or minimum calibrated age (i.e., the dates which bound formation of a feature).

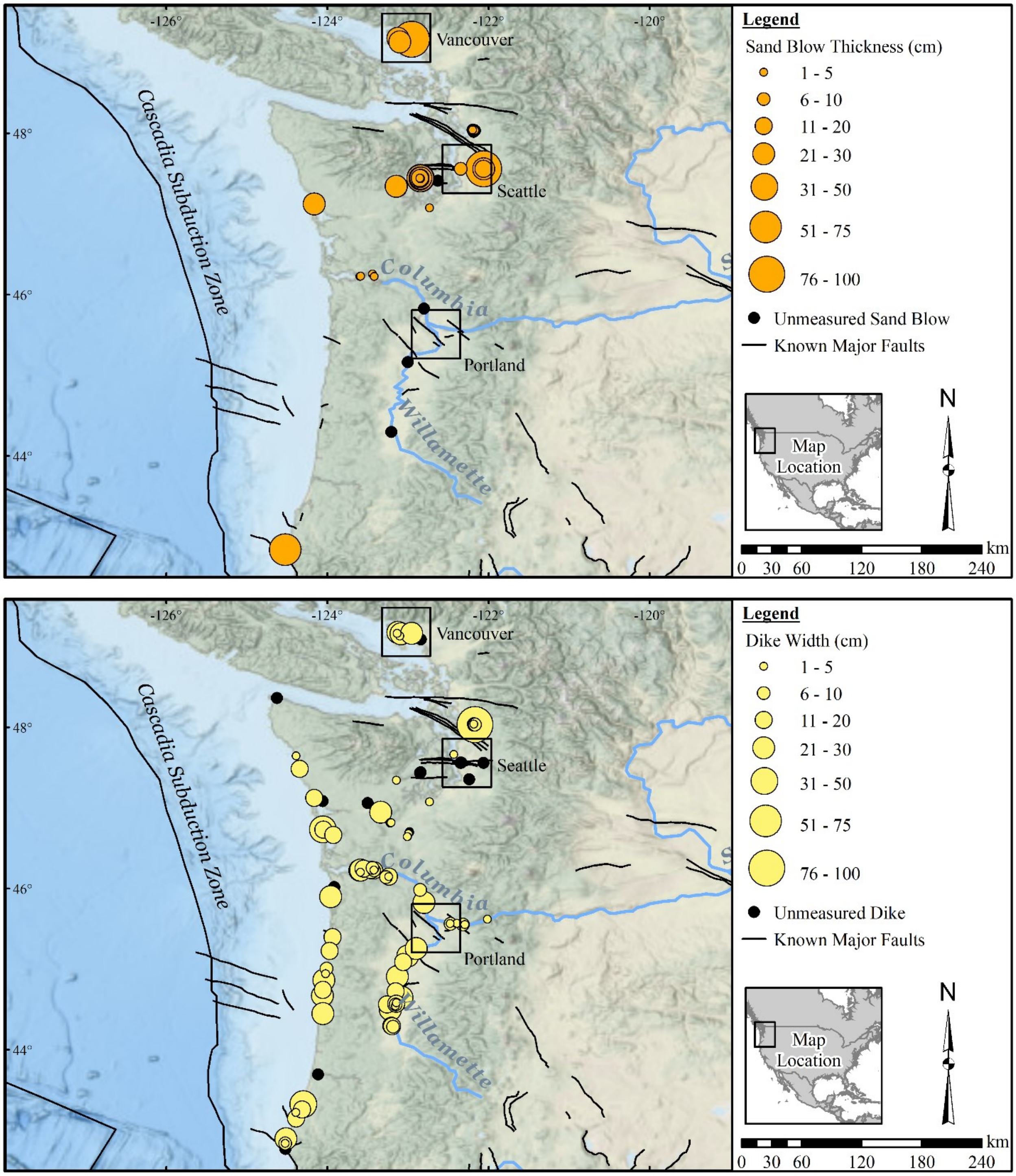

Fig. 5. Locations and sizes of paleoliquefaction features manifested as: (a) sand blows; and (b) dikes.

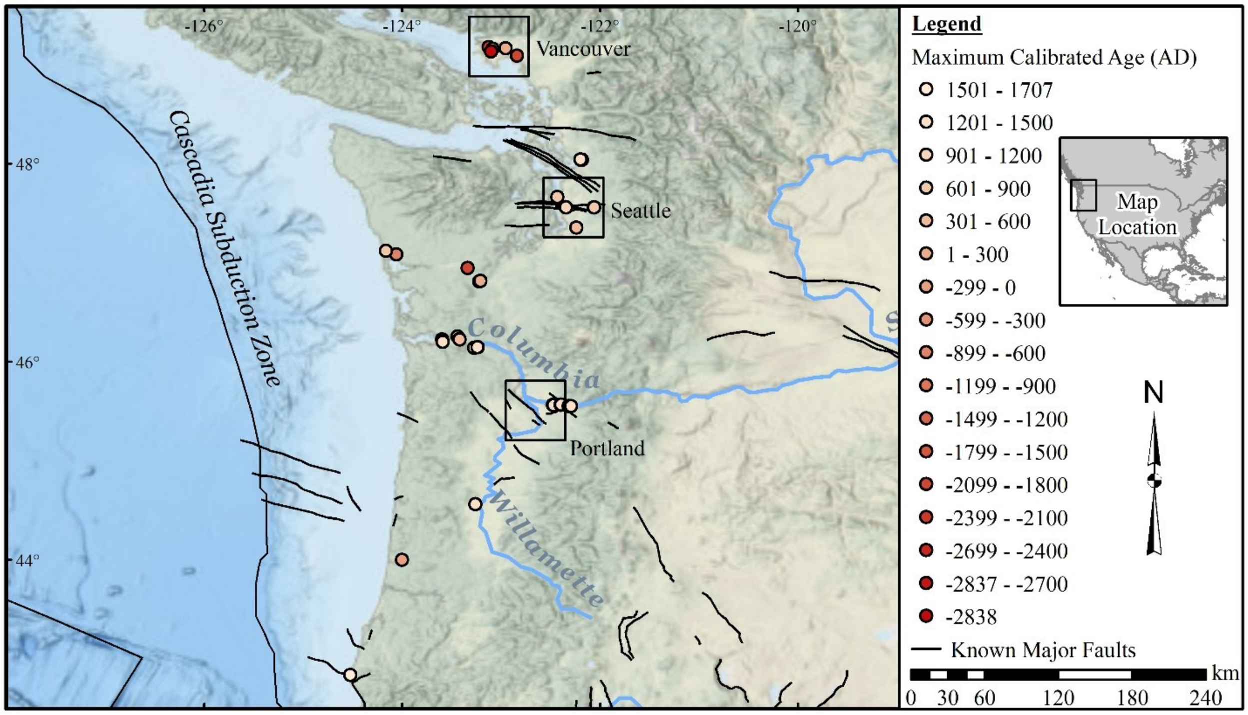

Fig. 6. Locations of paleoliquefaction features with dating information to constrain the maximum calibrated age (i.e., feature is younger than this date). Analogous figures can be developed to show the minimum calibrated age (i.e., feature is older than this date).

Of the 185 study sites compiled, 55 have liquefaction features with quantitatively constrained ages. Fig. 7 graphically depicts these constraints, juxtaposed against select historical earthquakes. Vertical lines denote the period in which a paleoliquefaction feature formed, with arrows denoting that either a minimum or maximum age is unknown. Superimposed are nine significant ruptures in the PNW, with emphasis on those which potentially could, or likely did, produce strong shaking where evidence was compiled. The constraints on these ruptures were collectively obtained from the paleoseismic studies of Atwater (1994, 1999), Satake et al. (1996), Atwater and Hemphill-Haley (1997), Atwater et al. (2003), and Kelsey et al. (2004). Other events proposed in the literature, such as the A.D. 770-1160 Tacoma fault rupture (Sherrod et al., 2004) and earlier ruptures in the CSZ, are not included. To this we also add the possibility of undocumented ruptures on faults known and unknown. While the age ranges of many features are relatively large (e.g., spanning multiple known earthquakes), several authors provide more narrow, preferred ages by holistically weighing the evidence at a site. In this regard, Fig. 7 does not attempt to convey the nuanced judgement of original investigators, but rather, serves as a preliminary guide for further reading. As an example, Davis (2019) investigated four neighboring sites on the Duwamish River in Seattle. While dating does not strictly bound the minimum ages (i.e., latest dates of formation) for many of the features investigated, Davis (2019) concluded:

"none of the dikes observed are likely to be as young as the 1700 Cascadia earthquake." Other authors similarly reject, or adopt, the plausibility of certain events to have caused a given feature. Some identify a particular causative event, such as the 1700 CSZ rupture (e.g., Atwater 1994; Satake et al., 1996) while others qualify a quantitative constraint, such as "slightly older than 130 B.C." or "significantly younger than 1150 B.C." (Obermeier, 1995). Preferred age estimates, and the rationale supporting them, are provided in the data attributes (see Table 3).

Ultimately, the compiled database may be used to target study sites for: (i) dating (e.g., where features are undated, or otherwise loosely constrained); and (ii) in-situ geotechnical tests, which are needed to perform inverse-analysis of the shaking experienced (See *Section 2.2*). Towards this end, the database notably lacks observations classified as negative (i.e., well documented sites judged capable of preserving evidence, but where none is observed), from which upper bounds on the intensity of shaking may be computed. While the aphorism "absence of evidence is not evidence of absence" holds true for all paleoseismic research, the need nonetheless exists, where prudent, to explicitly judge sites as "negative." While further field reconnaissance is undoubtedly needed in the PNW, to include focus on negative observations, such cases could at present be developed from the compiled database. That is, at sites observed to be susceptible to liquefaction and inferred to be capable of preserving evidence at a given time. As an example, liquefaction has yet to be tied to the 1700 CSZ rupture anywhere in the Puget Sound (i.e., the region between Seattle and Vancouver), despite there being numerous sites with recurrent liquefaction episodes. In total, 16 of the compiled study sites with age constraint – many located in the Puget Sound – are likely not to have liquefied in the 1700 CSZ rupture (or at least, no evidence has been found). In such cases, inverse-analyses would provide upper bounds on the intensity of shaking. Ultimately, regardless of whether sites are "positive" or "negative," a majority lack dating and geotechnical tests, which are both costly to perform, but which are needed to fully exploit the evidence. Accordingly, study sites should be selected for subsequent research in a strategic manner, guided by the compiled database (e.g., such that meaningful constraint on shaking intensity might be obtained).

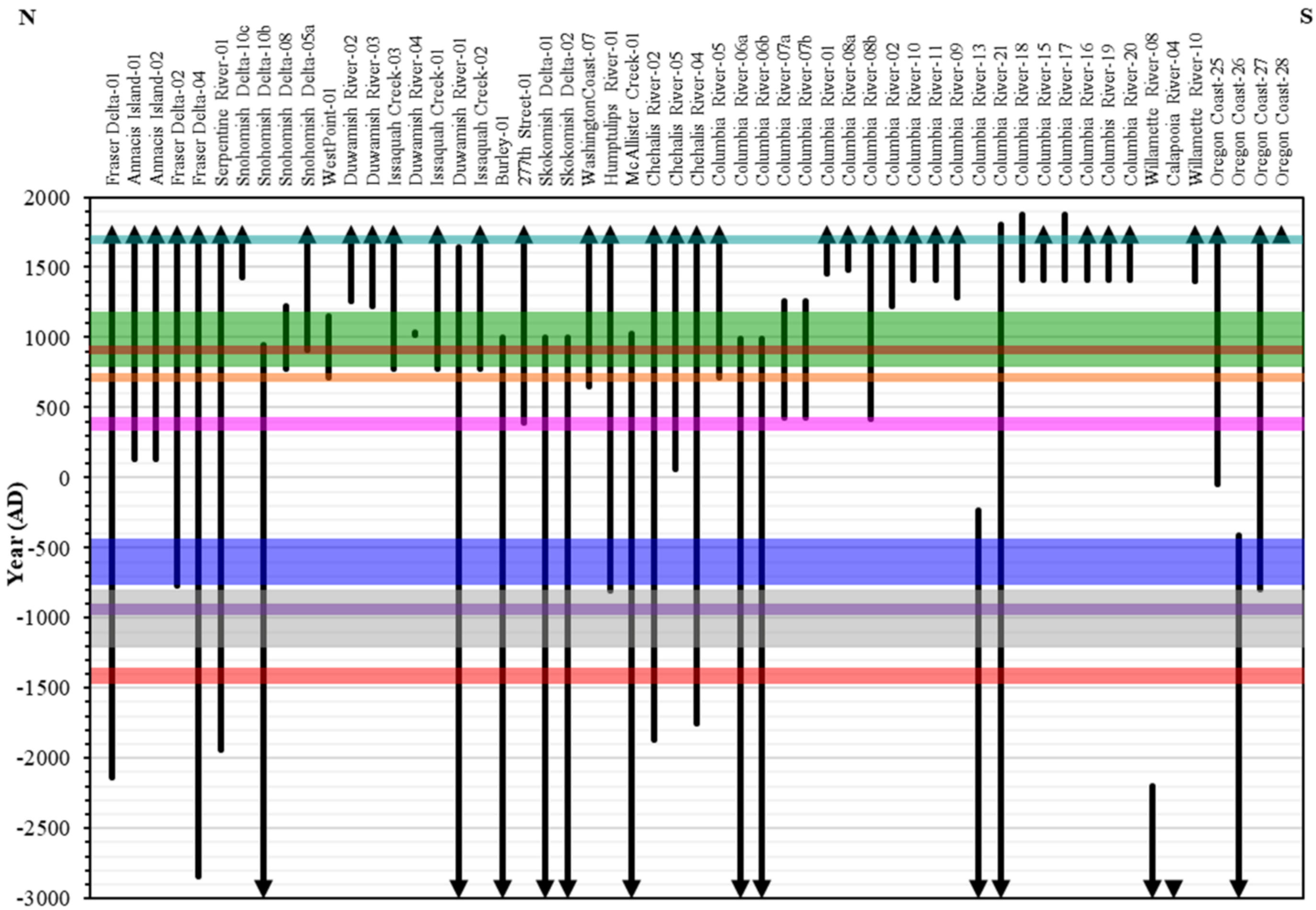

Event	Age Range	References
Cascadia Subduction Zone	AD 1700	Atwater (1994); Satake et al. (1996)
Cascadia Subduction Zone	AD 790 – 1180	Atwater and Hemphill-Haley (1997); Atwater et al. (2003)
Seattle Fault	AD 900 - 930	Atwater (1999)
Cascadia Subduction Zone	AD 700 - 730	Atwater and Hemphill-Haley (1997); Atwater et al. (2003)
Cascadia Subduction Zone	AD 350 - 420	Atwater and Hemphill-Haley (1997); Atwater et al. (2003)
Cascadia Subduction Zone	BC 760 - 450	Atwater and Hemphill-Haley (1997); Atwater et al. (2003)
Cascadia Subduction Zone	BC 980 - 900	Atwater and Hemphill-Haley (1997); Atwater et al. (2003)
Southern Whidbey Island Fault	BC 1200 - 800	Kelsey et al. (2004)
Cascadia Subduction Zone	BC 1450 - 1360	Atwater and Hemphill-Haley (1997); Atwater et al. (2003)

Fig. 7. Dating constraints on the formation of paleoliquefaction features at 55 study sites, juxtaposed against select, major earthquakes in the PNW. Study sites are identified on the horizontal axis and ordered from north to south; vertical lines denote the period in which a feature formed.

4. Forecasting CSZ Paleoliquefaction

In addition to further study of existing (i.e., published) paleoliquefaction sites, it is important that new sites be developed, to include geotechnical testing and analysis. As more sites are identified and analyzed, better constraint of regional ground-motions in past earthquakes will result. Yet, a field search of the entire PNW would be cost-prohibitive, and moreover, not all study sites will be of equal value. There are many locations where the presence or absence of liquefaction may do relatively little to constrain ground motions in a past event. For example, where: (i) the soil is unsusceptible to liquefaction, as is the case for most land; (ii) the soil is so susceptible to liquefaction that most ground-motion simulations predict liquefaction, even where motions differ; or (iii) most ground-motion simulations predict similar motions, and by corollary, lead to similar expectations of liquefaction. For field pursuits to be conducted more efficiently and strategically, it would be helpful to identify locations where uncertainties in ground-motion simulations (e.g., Frankel et al. 2018a; Wirth et al. 2018) give rise to differences in the forecasted liquefaction response. Accordingly, maps – specific to the CSZ – are next developed to prioritize where paleoliquefaction evidence should be searched for.

4.1 Geospatial Liquefaction Models

While liquefaction is most effectively forecasted using models based on in-situ geotechnical tests (e.g., Geyin and Maurer, 2020), such an approach is impractical at regional scale. As a result, regional maps of liquefaction hazard have traditionally been developed using geology maps, from which areal classifications of susceptibility are assumed. While this approach has been used in Cascadia (e.g., Palmer et al., 2007), it does not consider seismic loading, and thus, does not explicitly predict liquefaction. More recently, "geospatial" liquefaction models have been proposed for regional applications. In lieu of directly measuring subsurface traits, geospatial models attempt to infer below-ground conditions from above-ground parameters (e.g., metrics of surface slope, mineralogy, roughness, wetness, and reflectance; distance to and elevation above rivers, streams, and other water bodies; and various mapped or remotely sensed values describing geology, geomorphology, bedrock and water depth, hydrology, climate, etc.). In effect, these parameters serve as proxies of subsurface traits. The efficiency of one such model (Rashidan and Baise, 2020) has been shown, in some settings, to rival that of more sophisticated models based on subsurface test data (Geyin et al., 2020). In the 2001 Nisqually, Washington, earthquake, for example, it achieved 93% prediction efficiency when tested on all available field observations (Geyin et al., 2021). Accordingly, Rashidan and Baise (2020) will be adopted to compute the probability of liquefaction manifesting at the surface, defined as:

$$PoL(X) = \begin{cases} (1+e^{-X})^{-1} & if\ PGV > 3\frac{cm}{s}\ and\ PGA > 0.1\ g\ and\ V_{S30} < 620\ m/s \\ 0 & otherwise \end{cases} \quad (2)$$

Where: *PoL* is the probability of liquefaction manifesting within a 100 m by 100 m grid; *PGV* is peak ground velocity; *PGA* is peak ground acceleration; V_{S30} is the shear wave velocity time-averaged over the upper 30 m; and *X* is a series of model parameters and coefficients defined as:

$$X = 8.801 + 0.334\ln(PGV) - 1.918\ln(V_{s30}) + 0.0005408\,(precip) - 0.2054(d_w) - 0.0333(wtd) \quad (3)$$

In Eq. (3): *PGV* and V_{S30} are as previously defined; *precip* is the mean annual precipitation (mm) capped at 1700 mm; d_w is the closest distance (km) to a river or coastline; and *wtd* is the water table depth (m). Each of these inputs is readily available and was implemented exactly as described in Zhu et al. (2017) and Rashidan and Baise (2020). Specifically: V_{S30} was obtained from the Heath et al. (2020) global V_{S30} map; *precip* was obtained from the WorldClim database; *wtd* was obtained from the Fan et al. (2013) global water-depth map; and d_w was calculated using river and coastline data from the USGS HydroSHEDS database and the NOAA coastline dataset, respectively. These data sources are elaborated upon in the Data Availability section. In addition to *PoL*, Rashidan and Baise (2020) propose that the percent area of ground covered by liquefaction manifestation may be predicted as:

$$LSE(PoL) = 49.15\,(1 + 42.4e^{-9.165PoL})^{-2} \quad (4)$$

Where *LSE* is liquefaction spatial extent (%) and *PoL* was previously defined and calculated in Eqs. (2-3). Maps of both *PoL* and *LSE* will be generated for 30 different simulations of a CSZ earthquake.

4.2 CSZ Ground-Motion Simulations

Physics-based ground motion simulations, which explicitly model kinematic fault rupture, wave propagation, and the subsurface velocity structure, are especially useful for studying seismic sources that lack historic records, such as the CSZ. Physics-based simulations also help to elucidate and quantify complex phenomena that may go undetected by empirical observations at discrete stations (e.g., the effects of directivity, basins, and topography). Accordingly, Frankel et al. (2018a) and Wirth et al. (2018) developed 30 physics-based realizations of a full-fault M9 CSZ rupture. This suite of predictions includes variations in the hypocenter location, down-dip limit of fault rupture, slip distribution, and locations of asperities. The down-dip rupture extent was varied to be consistent with the logic tree adopted for the CSZ by Petersen et al. (2014) in the US National Seismic Hazard Map. For each scenario, a total of 500,000 motions were generated on a 1 km^2 spacing for a region ranging from Northern California to British Columbia, and from off the Pacific Coast to Central Washington and Oregon. The resulting motions can be retrieved from Frankel et al. (2018b) and have been used to forecast a variety of impacts on the built and living environment (e.g., Marafi et al., 2019, 2020).

4.3 Site-Response Analysis

Inherent to the Frankel et al. (2018a) and Wirth et al. (2018) suite of simulations is an assumed surficial shear-wave velocity (V_S) of 600 m/s. That is, the predictions are for rock conditions and do not consider the potential for local soil conditions to alter the amplitude and duration of incoming motions. Therefore, to predict liquefaction using the Rashidan and Baise (2020) model, the CSZ ground-motion simulations were first modified for surficial conditions using site-amplification factors derived from wave-propagation site-response analyses (i.e., to propagate the motions from rock through softer surficial materials, where present). Towards that end, profile measurements cannot feasibly be made everywhere, given the regional scale of the analyses. Accordingly, site amplification factors were computed, in part, using the Marafi et al. (2021) soil velocity model (SVM), which predicts profiles of V_S versus depth (z), and which is specific to the PNW. Using this approach, $V_S(z)$ is defined as:

$$V_s(z) = \begin{cases} V_{S0} & , \ z < 2.5\,m \\ V_{S0} + 1000 \cdot \left(k \frac{z-2.5}{Z_{1.0}-2.5}\right)^{\frac{1}{n}} & , \ z \geq 2.5\,m \end{cases} \tag{5}$$

where: V_{S0} defines V_S at the surface; k controls the near-surface rate-of-change in V_s; n controls the rate-of-change in V_s at greater depths; $Z_{1.0}$ is the depth, in meters, where V_S = 1 km/s; V_s and V_{S0} have units of m/s; and z is depth in meters. To anchor the predicted V_s at $Z_{1.0}$, the parameter k is defined as:

$$k = \left(\frac{1000 - V_{S0}}{1000}\right)^n \tag{6}$$

Thus, to apply Eqs. 5 and 6 at any given location requires input variable $Z_{1.0}$ and model parameters V_{S0} and n. Drawing from 909 V_S profiles measured in the Cascadia region, Marafi et al. (2021) modeled and trained expressions for V_{S0} and n:

$$V_{S0} = a_0 + a_1 (V_{S30})^{a_2} \tag{7}$$

$$n = b_0 (V_{S30})^{b_1} (Z_{1.0})^{b_2} (V_{S30} Z_{1.0})^{b_3} \tag{8}$$

where: a_0 = -629; a_1 = 434; a_2 = 0.122; b_0 = 0.00912; b_1 = 0.646; b_2= -0.201; b_3 = 0.136; and where other variables are as previously defined. While the training profiles were distributed throughout Washington, Oregon, and British Columbia, a majority were in the general vicinities of either Portland, Seattle, or Vancouver, consistent with both the extent and concentration of compiled paleoliquefaction study sites. For the present study, predictions of input variables $V_{S}30$ and $Z_{1.0}$ were obtained from the models of Heath et al. (2020) and Stephenson et al. (2017), respectively, as suggested by Marafi et al. (2021). The Stephenson et al. (2017) community velocity model provides mapping of deep geologic structure, but not of the near surface, and has a minimum V_S of 600 m/s. It thus provides the best means of estimating $Z_{1.0}$ but is otherwise unsuitable for predicting ground motions at the surface.

While V_S profile measurements are not yet available at paleoliquefaction sites, the adopted SVM was shown by Marafi et al. (2021) to provide significantly better predictions of profiles in the PNW across all site conditions, as compared to other regional or general SVMs. This may be attributable to Cascadia's numerous geologic basins and glaciated landscapes, which give rise to a wider range of V_{S30} and $Z_{1.0}$ combinations than is typically found in other data-rich seismic zones (e.g., California). Accordingly, the Marafi et al. (2021) SVM was used to estimate V_S profiles at 1 km^2 across a domain consistent with that of the CSZ ground-motion simulations.

Each of the 500,000 simulation motions, for each of 30 realizations, was modified via equivalent linear site-response analysis using pysra (Kottke, 2020), a Python implementation of the software Strata (Kottke and Rathje, 2008). Motions were input to the predicted profiles at a V_S of 600 m/s, consistent with the velocity at which they were computed. Nonlinear soil behavior was modeled per Darendeli (2001) with the following inputs: plasticity index = 30; unit weight = 19.6 kN/m^3; ground water depth = 5 m; coefficient of at-rest earth pressure = 1.0; and overconsolidation ratio computed per Wair et al. (2012). While systematic parameter variation was not undertaken, the most significant findings were relatively insensitive to the selected inputs, relative to other uncertainties (e.g., that of V_S versus depth). Ultimately, regional-scale analyses (i.e., analyses that do not use continuous subsurface measurements) have inevitable limitations and uncertainties. The Marafi et al. (2021) SVM is not a probabilistic model, nor are probabilistic estimates of its input parameters, V_{S30} and $Z_{1.0}$, available. The lack of uncertainty quantification within the methods for site-response and liquefaction should not be interpreted to mean that these and other uncertainties do not exist. As improved models of the subsurface velocity structure are developed, or as site-specific measurements are made, the accuracies of the site-response analyses performed herein will improve, and by corollary, so too will forecasts of consequent liquefaction.

Following the approach described above, ground surface time-histories were obtained with the same resolution and extents as the Frankel et al. (2018) and Wirth et al. (2018) simulations. For each of the 500,000 motions per realization, *PGV* and *PGA* were computed considering the geometric mean horizontal component of motion. These IMs were then linearly interpolated at a resolution of 100 m^2. Mapped in Fig. 8, considering all 30 realizations, is the 5-to-95 percentile variation in expected *PGA* and *PGV*. For many locations, these expected intensities vary significantly across the suite of realizations (e.g., differences in *PGA* exceeding 1.5 g) despite all modeling a M9 rupture. Some of the largest variations are seen: (i) on the Pacific Coast near the Juan de Fuca Strait in the north, and near Port Orford, OR, in the vicinity of the CSZ's terminus in the south (driven by differing assumed hypocenter locations, among other modeling variables); and (ii) where deep sediment basins have a propensity to amplify differences in incoming motions (e.g., in the vicinities of Portland, Seattle, and Vancouver). It can also be seen in Fig. 8 that some paleoliquefaction study sites are in areas of large ground-motion uncertainty. This hints at the possibility for the presence or absence of paleoliquefaction to constrain influential modeling variables, at least insofar as what occurred in A.D. 1700. In addition to the maps shown in Fig. 8, the median expected *PGA* and *PGV*, considering all 30 realizations, are mapped at full resolution in the Rasanen et al. (2021) GIS package, where the PNW paleoliquefaction database is also found. These predicted ground-motion intensities could be used to forecast a variety of regional-scale seismic impacts, in addition to liquefaction.

4.4 Results and Discussion

Liquefaction parameters *PoL* and *LSE* were forecasted across the PNW for each of the 30 modified ground-motion predictions resulting from *Section 4.3*. Given the uncertainties inherent to regional analyses, these products (i.e., liquefaction forecasts) should be viewed as preliminary tools: (i) to guide future field reconnaissance efforts and site-specific geotechnical studies, as will be further discussed; and (ii) to inform regional planning, policy, and science communication. As an example, *LSE* is mapped in Fig. 9 for one CSZ realization ("csz013"). It can be seen, for this realization, that some of the largest predicted *LSE* values are in the Fraser river delta of British Columbia. Notably, confirmed 1700 A.D. liquefaction has yet to be discovered anywhere in the vicinity, despite there being other, apparently older features at several study sites in the area. Thus, while site-specific geotechnical testing and analysis would be needed to confirm the geospatial model's prediction, the results in Fig. 9 might suggest that "csz013" is an unlikely realization of the motions experienced in 1700 A.D. Ultimately, geotechnical analyses at several regionally distributed study sites would be needed to conclude this.

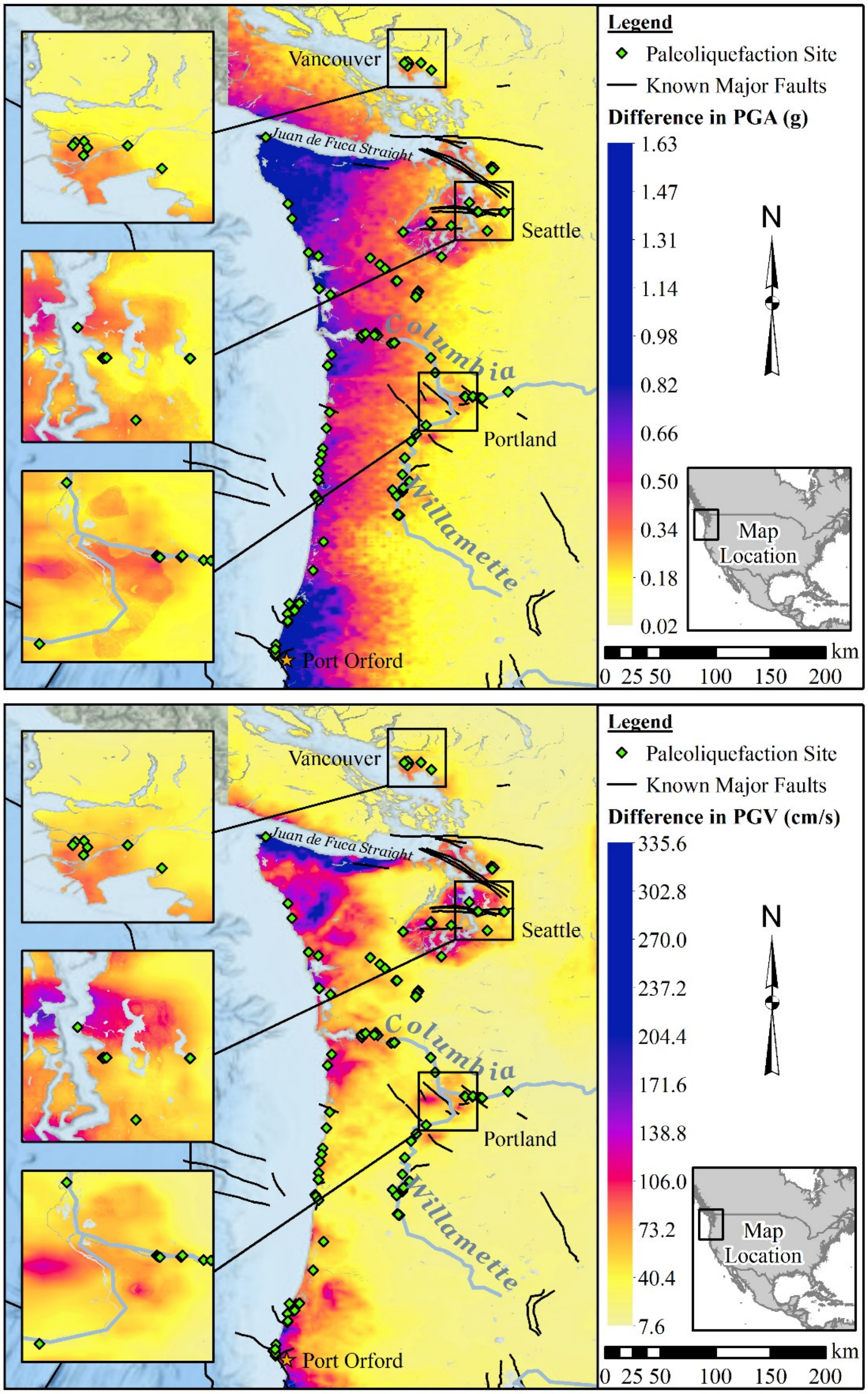

Fig. 8. Maps showing the 5-to-95 percentile variation in expected (a) *PGA* and (b) *PGV*, as computed from 30 different ground-motion simulations of a M9 CSZ earthquake. Expected shaking intensities vary significantly (e.g., by more than 1 g) depending on which simulation is adopted.

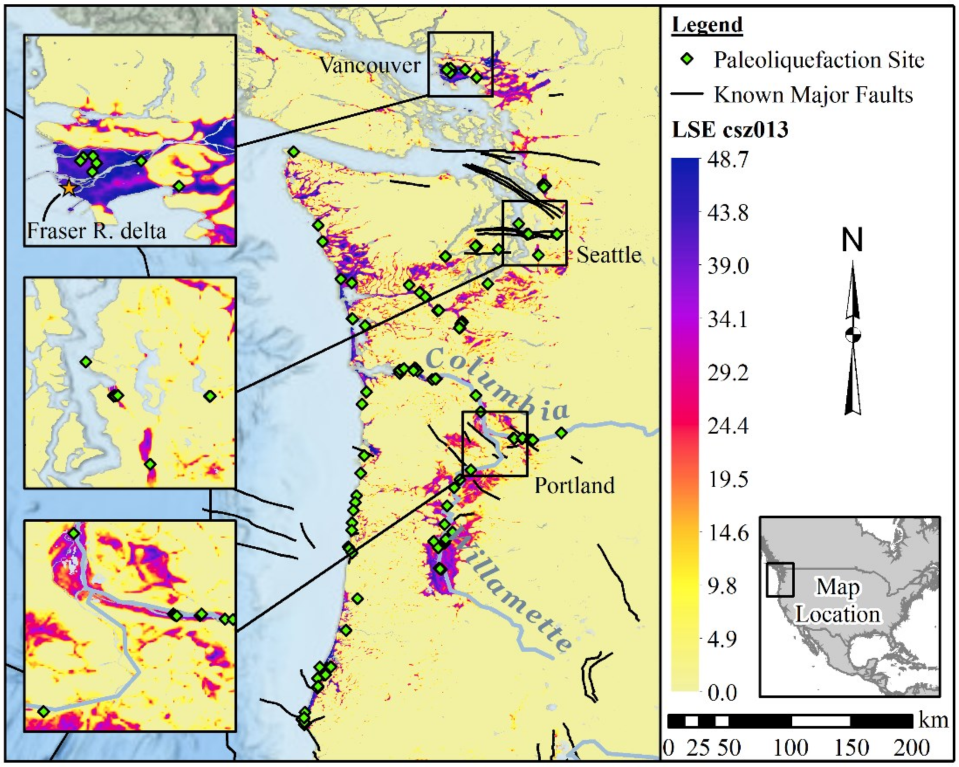

Fig. 9. Forecasted liquefaction spatial extent, *LSE* (%) computed for CSZ M9 ground-motion simulation "csz013" developed by Frankel et al. (2018a) and Wirth et al. (2018).

Analogous *PoL* and *LSE* forecasts are provided for each of the 30 CSZ M9 realizations, at full resolution, in the Rasanen et al. (2021) GIS package downloadable from https://doi.org/10.17603/ds2-fqkr-h615. Collectively, these forecasts may be used to identify locations: (i) where paleoliquefaction evidence is likely to be found; and (ii) where the expected liquefaction response differs across the suite of CSZ ground-motion realizations. As an example, the 5-to-95 percentile variation in *LSE*, considering all 30 realizations, is mapped in Fig. 10. Locations with large *LSE* differences are those where: (i) there are large differences in ground-motion intensity across realizations; and (ii) the subsurface is inferred to be susceptible to liquefaction. In this respect, differences in *LSE* increase as the inferred susceptibility to liquefaction increases, all else being equal. Fig. 10, which is included in the above GIS package, can thus be used to identify where the presence or absence of liquefaction would have greater potential to constrain the intensity of past shaking (i.e., where differences in *LSE* are greatest). In these locales, the presence or absence of features would be strongly at odds with some subset of the ground motion realizations, thereby diminishing their plausibility. Elsewhere, where differences in *LSE* are small, the presence or absence of features would potentially do little or nothing to constrain ground-motion models.

Regionally, some of the largest differences in *LSE* are (from south to north): near Klamath Lake, OR; along the Skagit River in the vicinity of Mt. Vernon, WA; and along the Fraser River in the vicinity of Chilliwack, BC. In each of these locales, predicted ground motions are sufficient for liquefaction in some realizations, assuming the subsurface is highly susceptible, but mechanistically insufficient in others, regardless of subsurface conditions. While paleoliquefaction has not been discovered in any of these areas, it is unknown whether field searches have been undertaken. Specific to the three urban centers highlighted in Fig. 10, relatively large *LSE* differences are predicted along the Columbia and Willamette Rivers in Portland, along the Duwamish River in Seattle, and in the Fraser River delta near Vancouver. In these urban areas, liquefaction manifestations are likely for some realizations of a CSZ rupture, but unlikely for others. Paleoliquefaction features have been documented in each of these urban areas, yet few, if any, of these were conceivably caused by the 1700 CSZ event (see Figure 7 and associated discussion). If these sites are judged not to have liquefied in 1700, the maximum shaking intensity could be provisionally constrained via geotechnical testing (i.e., if the intensity were any larger, liquefaction would be expected). Such analyses would also have the potential to inform regional ground-motion models, given that some subset of realizations would be less likely to represent that which occurred in 1700. Given the importance of geotechnical testing (e.g., CPTs) toward constraint of shaking intensity, an additional strategy is to search for the presence or absence of paleoliquefaction where testing has already been performed. That is, at locations where the subsurface is well documented, and where a significant cost of inverse analysis is already paid for. Towards this end, provided in the Rasanen et al. (2021) GIS package and mapped in Fig. 10, are the locations of many hundreds of CPTs presently available from the Washington Dept. of Natural Resources. Many of these CPTs, the data for which can be obtained from Jeschke et al. (2019), are in the vicinity of public lands and waterways where paleoliquefaction can be searched for.

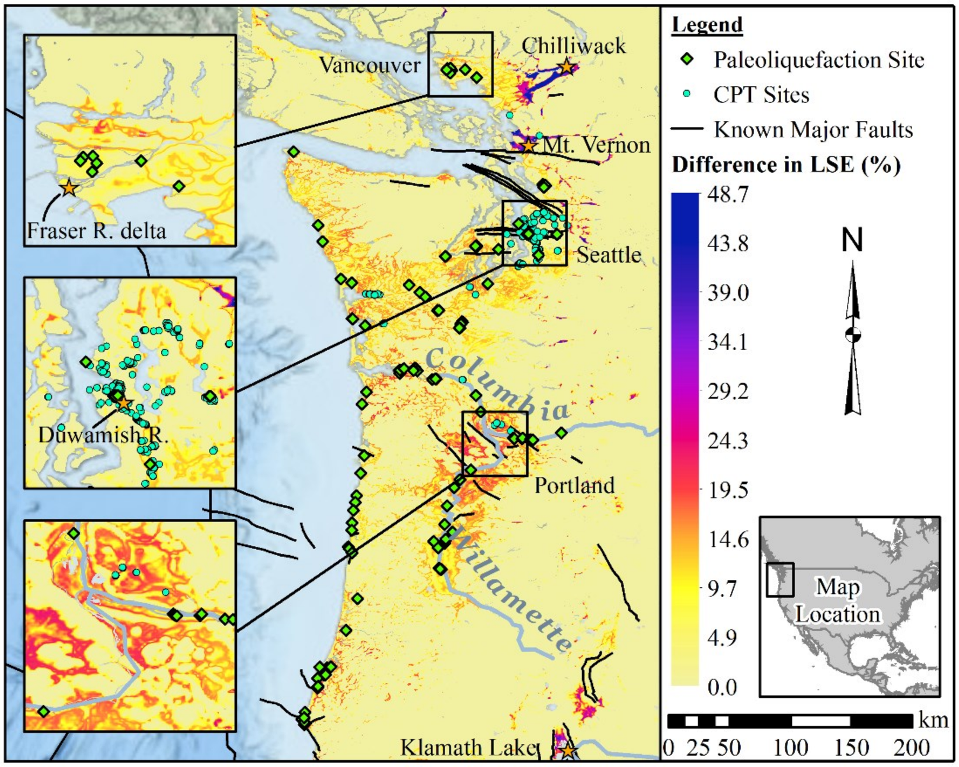

Fig. 10. The 5-to-95 percentile variation in expected *LSE*, as computed from 30 different ground-motion simulations of a M9 CSZ earthquake; paleoliquefaction and CPT sites are also mapped.

5. Conclusions

Paleoliquefaction provides the best, if not only, evidence from which the intensities of previous ground motions in the PNW may be constrained. Towards that ultimate goal, this paper first reviewed current paleoliquefaction inverse-analysis methods and their limited, prior applications in the PNW. Next, all existing PNW paleoliquefaction evidence was compiled from the literature into a GIS database for distribution to the engineering geology research community – the first such database compiled for the U.S. Pacific Northwest. This resulted in detailed data from 185 study sites (e.g., feature locations, types, sizes, and ages). Lastly, paleoliquefaction evidence was forecasted for 30 different physics-based ground motion simulations of a M9 CSZ earthquake. Collectively, these maps can be used to guide field explorations by engineering geologists for new evidence, considering both: (i) where evidence is likely to be found; and (ii) whether evidence is likely to provide meaning constraint of CSZ ground motion models. Of additional utility, this process resulted in the first ever suite of M9 CSZ ground-motion predictions for the Cascadia Region. In making these predictions, wave-propagation based site-response analyses were used to account for expected near-surface site effects. Together, the maps of expected shaking intensity and liquefaction may be useful in regional loss estimation, scenario planning, and science communication. Ultimately, as more paleoliquefaction evidence is identified and analyzed, better constraint of regional ground-motions in past earthquakes will result. This will undoubtedly require unified collaboration between geoscientists, geoengineers, and other research professionals. The products presented herein form a foundation for these efforts.

6. Data Availability

Available in digital format from NEHRI DesignSafe (https://doi.org/10.17603/ds2-fqkr-h615) (Rasanen et al., 2021) are the: (i) PNW paleoliquefaction database; (ii) maps showing the predicted median and variance of *PGA* and *PGV* across 30 simulations of a CSZ earthquake; (iii) maps of forecasted *PoL* and *LSE* for 30 simulated CSZ earthquakes; and (iv) locations of existing CPTs, as discussed in the text. In addition, all inputs required of the Rashidan and Baise (2020) geospatial liquefaction model are globally available. Distance to river was computed from the Hydrological data and maps based on Shuttle Elevation Derivatives at multiple Scales (HydroSHEDS) database (https://www.hydrosheds.org/page/hydrorivers, accessed July 2019). Distance to coast was computed from the National Oceanic and Atmospheric Administration coastline dataset (https://shoreline.noaa.gov/data/datasheets/medres.html, accessed July 2019). Mean annual precipitation was obtained from the WorldClim database (https://worldclim.org/, accessed July 2019).

7. Acknowledgements

The presented study is based on work supported by the National Science Foundation (NSF) under Grant No. CMMI-1751216, by the NSF Graduate Research Fellowship Program under Grant No. DGE-1762114, and by the University of Washington Royalty Research Fund (RRF). However, any opinions, findings, and conclusions or recommendations expressed in this paper are those of the authors and do not necessarily reflect the views of the NSF or RRF.

8. References

Allen, T.I. and Wald, D.J. (2009). "On the use of high-resolution topographic data as a proxy for seismic site conditions (Vs30)." *Bulletin of the Seismological Society of America* 99(2A): 935-943.

Ambrayses, N.N. (1988). "Engineering seismology." *Earthquake Eng and Structural Dynamics* 17: 1-105.

Atwater, B.F. (1992). "Geologic Evidence for Earthquakes During the Past 2000 Years Along the Copalis River, Southern Coastal Washington." *Journal of Geophysical Research* 97(B2): 1901-1919.

Atwater, B.F. (compiler) (1994). "Geology of Holocene liquefaction features along the lower Columbia River at Marsh, Brush, Price, Hunting, and Wallace Islands, Oregon and Washington." *U.S. Geol. Surv. OpenFile Rept.* 94-209, 30 pp.

Atwater, B.F. (1999). "Radiocarbon dating of a Seattle earthquake to A.D. 900–930." *SRL* 70: 232.

Atwater, B.F., and Hemphill-Haley, E. (1997). “Recurrence Intervals for Great Earthquakes of the Past 3,500 Years at Northeastern Willapa Bay, Washington.” *U.S. Geological Survey Paper 1576.*

Atwater, B.F., Stuiver, M., and Yamaguchi, D.K. (1991). “Radiocarbon test of earthquake magnitude at the Cascadia subduction zone.” *Nature* 353: 156-158.

Atwater, B.F., Carson, B., Griggs, G.B., Johnson, H.P., and Salmi, M.S. (2014). “Rethinking turbidite paleoseismology along the Cascadia subduction zone.” *Geology* 42(9): 827-830.

Atwater, B.F., Tuttle, M.P., Schweig, E.S., Rubin, C.M., Yamaguchi, D.K., and Hemphill-Haley, E. (2003). “Earthquake recurrence inferred from paleoseismology.” *Developments in Quaternary Science* 1: 331-348.

Aydan, O., Ulusay, R., Kumsar, H., and Tuncay, E. (2000). “Site investigation and engineering evaluation of the Duzce-Bolu earthquake of November 12, 1999.” *Turkish Earthquake Foundation, Istanbul*. Report No. TDV/DR 09-51, 307 p.

Bastin, S., Bassett, K., Quigley, M.C., Maurer, B.W., Green, R.A., Bradley, B.A., and Jacobson, D. (2016). “Late Holocene liquefaction at sites of contemporary liquefaction during the 2010-2011 Canterbury Earthquake Sequence.” *Bulletin of the Seismological Society of America* 106(3): 881-903.

Bourgeois, J., and Johnson, S.Y. (2001). “Geologic evidence of earthquakes at the Snohomish delta, Washington, in the past 1200 yr.” *Geological Society of America Bulletin* 113(4): 482-494.

Briggs, G.G. (1994). "Coastal Crossing of the Elastic Strain Zero-Isobase, Cascadia Margin, South Central Oregon Coast.” *Dissertations and Theses*. Paper 4739.

Castilla, R.A. and Audemard, F.A. (2007). “Sand blows as a potential tool for magnitude estimation of pre-instrumental earthquakes.” *Journal of Seismology* 11: 473-487.

Clague, J.J., Naesgaard, E., and Sy, A. (1992). “Liquefaction features on the Fraser delta: evidence for prehistoric earthquakes?” *Canadian Journal of Earth Sciences* 29: 1734.1745.

Clague, J.J., Naesgaard, E., and Nelson, A.R. (1997). “Age and significance of earthquake-induced liquefaction near Vancouver, British Columbia, Canada.” *Can. Geotech. J.* 34: 53-62.

Cox, R.T., Hill, A.A., Larsen, D., Holzer, T., Forman, S.L., Noce, T., Gardner, C., and Morat, J. (2007). “Seismotectonic implications of sand blows in the southern Mississippi Embayment.” *Engineering* Geology 89: 278-299.

Darendeli, M. B. (2001). “Development of a new family of normalized modulus reduction and material damping curves.” PhD Dissertation, Dept. of Civil Engineering, University of Texas at Austin.

Davis, E. (2019). “Seattle liquefaction features along the Duwamish Waterway, Washington.” *Seismological Society of America Annual Meeting*, 23-26 April, Seattle, USA.

de Magistris, F. S., Lanzano, G., Forte, G., & Fabbrocino, G. (2013). “A database for PGA threshold in liquefaction occurrence.” *Soil Dynamics and Earthquake Engineering*, 54: 17-19.

Engelhart, S.E., Horton, B.P., Nelson, A.R., Hawkes, A.D., Witter, R.C., Wang, K., Wang, P.-L., and Vane, C.H. (2013). “Testing the use of microfossils to reconstruct great earthquakes at Cascadia.” *Geology* 41 (10): 1067–1070.

Fan, Y., Li, H., and Miguez-Macho, G. (2013). “Global patterns of groundwater table depth.” *Science* 339: 940 943.

Fiedorowicz, B.K. (1997). “Geologic Evidence of Historic and Preshistoric Tsunami Inundation at Seaside, Oregon.” *M.S. Thesis*, Portland State University, Portland.

Frankel, A., Wirth, E., Marafi, N., Vidale, J., and Stephenson, W. (2018a). “Broadband Synthetic Seismograms for Magnitude 9 Earthquakes on the Cascadia Megathrust Based On 3D Simulations and Stochastic Synthetics (Part 1): Methodology and Overall Results.” *Bulletin of the Seismological Society of America* 108 (5A): 2347-2369.

Frankel, A., Wirth, E., and Marafi, N. (2018b). "The M9 Project Ground Motions." DesignSafe-CI. https://doi.org/10.17603/DS2WM3W.
Galli, P. (2000). "New empirical relationships between magnitude and distance for liquefaction." *Tectonophysics* 324: 169-187.
Geyin, M. and Maurer, B.W. (2020). "Fragility functions for liquefaction-induced ground failure." *Journal of Geotechnical and Geoenvironmental Engineering* 146(12): 04020142.
Geyin, M., Baird, A.J., and Maurer, B.W. (2020). "Field assessment of liquefaction prediction models based on geotechnical vs. geospatial data, with lessons for each." *Earthquake Spectra* 36(3): 1386–1411.
Geyin, M., Maurer, B.W., and Christofferson, K. (2021). "An AI-Driven, Mechanistically Grounded Geospatial Liquefaction Model for Rapid Response and Planning." *Soil Dynamics and Earthquake Eng., In Review.*
Gheibi, E., Gassman, S., & Talwani, P. (2020). "Regional assessment of prehistoric earthquake magnitudes in the South Carolina Coastal Plain." *Bulletin of Eng Geology and the Environment 79*(3): 1413-1427.
Goldfinger, C., Nelson, C.H., Morey, A.E., Johnson, J.E., Patton, J.R., Karabanov, E., Gutiérrez-Pastor, J., Eriksson, A.T., Gràcia, E., Dunhill, G., Enkin, R.J., Dallimore, A., and Vallier, T., (2012). "Turbidite event history - methods and implications for Holocene paleoseismicity of the Cascadia subduction zone." *U.S. Geological Survey Professional Paper 1661–F*, 170 pg.
Green, R.A., Olson, S.M., and Obermeier, S.F. (2005). "Geotechnical analysis of paleoseismic shaking using liquefaction effects: field examples." *Engineering Geology* 76: 263-293.
Green, R.A., Maurer, B.W., Bradley, B.A., Wotherspoon, L., and Cubrinovski, M. (2014). "Implications from liquefaction observations in New Zealand for interpreting paleoliquefaction data in the central eastern United States." U.S. Geological Society Technical Report G12AP20002, 97pp.
Green, R.A., Bommer, J.J., Rodriguez-Marek, A., Maurer, B.W., Stafford, P.J., Edwards, B., Kruiver, P.P., De Lange, G. and Van Elk, J. (2019). "Addressing limitations in existing 'simplified' liquefaction triggering evaluation procedures: application to induced seismicity in the Groningen gas field." *Bulletin of Earthquake Engineering* 17(8): 4539-4557.
Hayati, H. and Andrus, R.D. (2008). "Liquefaction potential map of Charleston, South Carolina base on the 1886 earthquake." *Journal of Geotechnical and Geoenvironmental Engineering* 134(6): 815-828.
Heath, D., Wald, D. J., Worden, C. B., Thompson, E. M., and Smoczyk, G. (2020). "A Global Hybrid VS30 Map with a Topographic-Slope-Based Default and Regional Map Insets." *Earthquake Spectra* 36(3): 1570-1584.
Holzer, T.L., Noce, T.E., and Bennett, M.J. (2015). "Strong ground motion inferred from liquefaction caused by the 1811-1812 New Madrid, Missouri, Earthquakes." *Bulletin of the Seismological Society of America* 105(5): 2589-2603.
Hu, K., Gassman, S.L., and Talwani, P. (2002). "Magnitudes of prehistoric earthquakes in the South Carolina Coastal Plain from geotechnical data." *Seismological Research Letters* 73(6): 979-991.
Ishihara, K. (1985). "Stability of natural deposits during earthquakes." In *International conference on soil mechanics and foundation engineering. 11* (pp. 321-376).
Iwasaki, T., Tatsuoka, F., Tokida, K., and Yasud, S. (1978). "A practical method for assessing soil liquefaction potential based on case studies at various sites in Japan." *2nd Intl Conf. Microzonation*.
Jeschke, D. A.; Eungard, D. W.; Troost, K. G.; Wisher, A. P, (2019). "Subsurface database of Washington State - GIS data." *Washington Geological Survey Digital Data Series 11, version 2.1*, previously released August 2017 [http://www.dnr.wa.gov/publications/ger_portal_subsurface_database.zip].
Kelsey, H.M., Witter, R.C., Hemphill-Haley, E. (2002). "Plate-boundary earthquakes and tsunamis of the past 5500 yr, Sixes River estuary, southern Oregon. *GSA Bulletin* 114(3): 298-314.

Kelsey, H.M., Sherrod, B., Johnson, S.Y., and Dadisman, S.V. (2004). "Land-level changes from a late Holocene earthquake in the northern Puget Lowland, Washington." *Geological Society of America* 32(6): 469-472.

Kottke, A.R. and Rathje, E.M. (2008). "Technical manual for Strata." Report No.: 2008/10. Pacific earthquake engineering research center. Berkeley: University of California.

Kottke, A.R. (2020). "Site response analysis for Python." https://doi.org/10.5281/ zenodo.3522104. https://github.com/arkottke/pysra. Accessed 1 Feb 2020.

Kuribayahsi, E. and Tatsuoka, F. (1975). "Brief review of liquefaction during earthquakes in Japan." *Soils and Foundations* 15(4): 81-92.

Marafi, N.A., Eberhard, M.O., Berman, J.W., Wirth, E.A., and Frankel, A.D. (2019). "Impacts of simulated M9 Cascadia subduction zone motions on idealized systems." *Earthquake Spectra 35*(3), 1261-1287.

Marafi, N.A., Makdisi, A.J., Eberhard, M.O., & Berman, J.W. (2020). "Impacts of an M9 Cascadia Subduction Zone Earthquake and Seattle Basin on Performance of RC Core Wall Buildings." *Journal of Structural Engineering* 146(2), 04019201.

Marafi, N. A., Grant, A., Maurer, B. W., Rateria, G., Eberhard, M. O., & Berman, J. W. (2021). "A generic soil velocity model that accounts for near-surface conditions and deeper geologic structure." *Soil Dynamics and Earthquake Engineering 140*: 106461.

Martin, J.R. and Clough, G.W. (1990). "Implications from a geotechnical investigation of liquefaction phenomena associated with seismic events in the Charleston, SC area." Report to USGS Grant No. 14-08-001-G-1348, Virginia Tech, Blacksburg, VA, 414 p.

Martin, M.A., and Bourgeois, J. (2012). "Vented sediments and tsunami deposits in the Puget Lowland, Washington – differentiating sedimentary processes." *Sedimentology* 59: 419-444.

Maurer, B.W., Green, R.A., Quigley, M.C. and Bastin, S. (2015a). "Development of magnitude-bound relations for paleoliquefaction analyses: New Zealand case study." *Engineering Geology* 197: 253-266.

Maurer, B.W., Green, R.A. and Taylor, O.D.S. (2015b). "Moving towards an improved index for assessing liquefaction hazard: lessons from historical data." *Soils and Foundations* 55(4): 778-787.

Maurer, B.W., Green, R.A., Cubrinovski, M., and Bradley, B. (2015c). "Assessment of CPT-based methods for liquefaction evaluation in a liquefaction potential index framework." *Géotechnique* 65(5): 328-336.

Maurer, B.W., Green, R.A., Wotherspoon, L.M. & Bastin, S. (2019). "The stratigraphy of compound sand blows at sites of recurrent liquefaction: implications for paleoseismicity studies." *Earthquake Spectra* 35(3): 1421-1440.

National Research Council (NRC) (2016). "State of the art and practice in the assessment of earthquake induced soil liquefaction and its consequences." committee on earthquake induced soil liquefaction assessment (Edward Kavazanjian, Jr., Chair, Jose E. Andrade, Kandian "Arul" Arulmoli, Brian F. Atwater, John T. Christian, Russell A. Green, Steven L. Kramer, Lelio Mejia, James K. Mitchell, Ellen Rathje, James R. Rice, and Yumie Wang), The National Academies Press, Washington, DC.

Nuclear Regulatory Commission (NRC) (2012). "Central and Eastern United States Seismic Source Characterization for Nuclear Facilities." Tech.Rep.NUREG-2115, NRC, Rockville, MD.

O'Donnell III, R.J., Hawkes, A.D., Lane, C.S., Engelhard, S.E., Horton, B.P., Bobrowsky, P., Sawai, Y., Witter, R.C., Nelson, A.R., and Tanigawa, K. (2017). "Assessing the utility of δ13C and bulk geochemistry in estuaries along the Cascadia subduction zone for coastal paleoseismology." *Geological Society of America Abstracts with Programs* 49(6): 58-2.

Obermeier, S. F. (1995). "Preliminary estimates of the strength of prehistoric shaking in the Columbia River Valley and the southern half of coastal Washington, with emphasis for a Cascadia Subduction Zone earthquake about 300 years ago." *U.S. Geol. Surv.* Open-File Rept. 94-589, 46 pp.

Obermeier, S. F. (1996). “Use of liquefaction-induced features for paleoseismic analysis—an overview of how seismic liquefaction features can be distinguished from other features and how their regional distribution and properties of source sediment can be used to infer the location and strength of Holocene paleo-earthquakes.” *Engineering Geology*, *44*(1-4): 1-76.

Obermeier, S.F. and Dickenson, S.E. (2000). “Liquefaction evidence for the strength of ground motions resulting from late Holocene Cascadia subduction earthquakes, with emphasis on the event of 1700 A.D.” *Bulletin of the Seismological Society of America* 90(4): 876-896.

Obermeier, S.F., Pond, E.C., Olsen, S.M. with contributions by Green, R.A, Mitchell, J.K., and Stark, T.D. (2001). “Paleoliquefaction studies in continental settings: geologic and geotechnical factors in interpretations and back-analysis.” U.S. Geological Survey Open-File Report 01–029.

Obermeier, S.F., Olson, S.M. and Green, R.A (2005). “Field occurrences of liquefaction-induced features: a primer for engineering and geologic analysis of paleoseismic shaking.” *Engineering Geology* 76: 209-234.

Obermeier, S.F., Olson, S.M., Green, R.A., Schweig, E., and Williams, R. (2011). “Clastic dikes and ground fractures; seismic or not?” *Seismological Research Letters* 82: 335.

Olson, S.M., Green, R.A. and Obermeier, S.F. (2005a). “Revised magnitude bound relation for the Wabash valley seismic zone of the central United States.” *Seismological Research Letters* 76(6): 756–771.

Olson, S.M., Green, R.A. and Obermeier, S.F. (2005b). “Geotechnical analysis of paleoseismic shaking using liquefaction features: a major updating.” *Engineering Geology* 76: 235–261.

Palmer, S.P., Magsino, S.L., Bilderback, E.L., Poelstra, J.L., Folger, D.S.; Niggemann, R.A. (2007). “Liquefaction susceptibility and site class maps of Washington State, by county.” *Washington Division of Geology and Earth Resources Open File Report 2004-20*.

Papadopoulos, G.A. and Lefkopoulos, G. (1993). “Magnitude-distance relations for liquefaction in soil from earthquakes.” *Bulletin of the Seismological Society of America* 83(3): 925-938.

Papathanassiou, G., Pavlides, S., Christaras, B. and Pitilakis, K. (2005). “Liquefaction case histories and empirical relations of earthquake magnitude versus distance from the broader Aegean region.” *Journal of Geodynamics* 40: 257-278.

Peters, R., Jaffe, B., and Gelfenbaum, G. (2007). “Distribution and sedimentary characteristics of tsunami deposits along the Cascadia margin of western North America.” *Sed Geo* 200: 372-386.

Petersen, M.D., Moschetti, M.P., Powers, P.M., Mueller, C.S., Haller, K.M., Frankel, A.D., Zeng, Y., Rezaeian, S., Harmsen, S.C., Boyd, O.S., Field, N., Chen, R., Rukstales, K.S., Luco, N., Wheeler, R.L., Williams, R.A. and Olsen, A.H. (2014). “Documentation for the 2014 update of the United States national seismic hazard maps.” USGS Open-File Report 2014–1091, 243 p.

Peterson C.D. and Madin, I.P. (1997). “Coseismic Paleoliquefaction Evidence in the Central Cascadia Margin, USA.” *Oregon Geology* 59, 51-74.

Peterson, C.D., Cruikshank, K.M., Jol, H.M. and Schilichting, R.B. (2008). “Minimum Runup Heights of Paleotsunami from Evidence of Sand Ridge Overtopping at Cannon Beach, Oregon, Central Cascadia Margin, USA.” *Journal of Sedimentary Research* 78: 390-409. http://dx.doi.org/10.2110/jsr.2008.044

Peterson, C.D., Cruikshank, K.M., Darienzo, M.E., Wessen, G., Butler, V. and Sterling, S. (2013). “Coseismic Subsidence and Paleotsunami Runup Records from Latest Holocene Deposits in the Waatch Valley, Neah Bay, Northwest Washington, USA: Links to Great Earthquakes in the Northern Cascadia Margin.” *Journal of Coastal Research*, 29, 157-172. http://dx.doi.org/10.2112/JCOASTRES-D-12-00031.1

Peterson, C.D., et al. (2014). “Large-Scale Fluidization Features from Late Holocene Coseismic Paleoliquefaction in the Willamette River Forearc Valley, Central Cascadia Subduction Zone, Oregon, USA.” *Open Journal of Earthquake Research*, 3: 82-99

Peterson, C.D., Jol, H.M. and Alldritt, K. (2005). "Reconnaissance Subsurface Investigation of Bandon Marsh, Oregon." U.S. Fish and Wildlife Service, Newport.

Pirrotta, C., Barbano, M.S., Guarnieri, P. and Gerardi, F. (2007). "A new dataset and empirical relationships between magnitude/intensity and epicentral distance for liquefaction in central-eastern Sicily." *Annals of Geophysics* 50(6): 763-774.

Polenz, M., Czajkowski, J.L., Paulin, G.L., Contreras, T.A., Miller, B.A., Martin, M.E., Walsh, T.J., Logan, R.L., Carson, R.J., Johnson, C.N., Skov, R.H., Mahan, S.A., Cohan, C.R. (2010). "Geological Map of the Skokomish Valley and Union 7.5-minute Quadrangles, Mason County, Washington. *Washington Division of Geology and Earth Resources* Open File Report 2010-3, 1 sheet, scale 1:24,000, with 21 p. text.

Quigley, M.C., Bastin, S., Bradley, B.A. (2013). "Recurrent liquefaction in Christchurch, New Zealand, during the Canterbury earthquake sequence." *Geology* 41: 419–422.

Rasanen, R., Marafi, N.A., and Maurer, B.W. (2021). "Compilation and Forecasting of Paleoliquefaction Evidence for the Strength of Ground Motions in the U.S. Pacific Northwest: A Digital Dataset (Version 2)." DesignSafe-CI. https://doi.org/10.17603/ds2-fqkr-h615.

Rasanen, R., and Maurer, B.W. (2021). "Probabilistic seismic source location and magnitude via inverse analysis of liquefaction evidence." *Earthquake Spectra*, In Review, Elsevier.

Rashidian, V., and Baise, L.G. (2020). "Regional efficacy of a global geospatial liquefaction model." *Engineering Geology* 272: 105644.

Rodriguez-Marek, A., and Ciani, D. (2008). "Probabilistic methodology for the analysis of paleoliquefaction features." *Engineering Geology* 96(3): 159-172.

Satake, K., Shimazaki, K., Tsuji, Y. & Ueda, K. (1996). "Time and size of a giant earthquake in Cascadia inferred from Japanese tsunami record of January 1700." *Nature* 379, 246–249.

Sherrod, B.L. (2001). "Evidence for earthquake-induced subsidence about 1100 yr ago in coastal marches of southern Puget Sound, Washington." *Geo Soc of America Bull* 113(10): 1299-1311.

Sherrod, B., Brocher, T.M., Weaver, C.S., Bucknam, R.C., Blakely, R.J., Kelsey, H.M., Nelson, A.R., Haugerud, R. (2004). "Holocene fault scarps near Tacoma, Washington, USA." *Geological Society of America* 32(1): 9-12.

Sims, J.D. & Garvin, C.D. (1995). "Recurrent liquefaction induced by the 1989 Loma Prieta earthquake and 1990 and 1991 aftershocks: implications for paleoseismicity studies." *Bulletin of the Seismological Society of America* 85(1): 51-65.

Sims, J.D. (2002). "Paleoliquefaction Study of the Willamette River Valley, Portland to Corvallis, Oregon." *US Geological Survey*, Reston, Element II under Contract 02HQGR0021

Stephenson, W.J., Reitman, N.G., and Angster, S.J., (2017). "P- and S-wave velocity models incorporating the Cascadia subduction zone for 3D earthquake ground motion simulations, version 1.6." *U.S. Geological Survey Open-File Repo*rt 2017–1152, 17 p., https://doi.org/10.3133/ofr20171152.

Struble, W., Roering, J., Burns, W.J., Black, B., Calhoun, N., and Wetherell, L.R. (2017). "Propensity for deep-seated landslides in the Oregon coastal ranges during Cascadia megathrust earthquake through dendrochronological dating of landslide-dammed lakes." *GSA Abstracts* 49(6): 58-7.

Stuiver, M., Reimer, P.J., and Reimer, R.W. (2020). CALIB 7.1 [WWW program] at http://calib.org, accessed 2020-3-18.

Takada, K. and Atwater, B.F. (2004). "Evidence for Liquefaction Identified in Peeled Slices of Holocene Deposits along the Lower Columbia River, Washington." *BSSA* 94: 550-575.

Talwani, P. and Schaeffer, W.T. (2001). "Recurrence rates of large earthquakes in the South Carolina coastal plain based on paleoliquefaction data." *Journal of Geophysical Research* 106: 6621-6642.

Thrush, C., and Ludwin, R.S. (2007). "Finding fault: Indigenous seismology, colonial science, and the rediscovery of earthquakes and tsunamis in Cascadia." *American Indian Culture and Res J* 31(4): 1-24.

Tuttle, M.P. (2001). "The use of liquefaction features in paleoseismology: lessons learned in the New Madrid seismic zone, central United States." *Journal of Seismology* 5: 361-380.

Tuttle, M. and Hartleb, R. (2012). "CEUS Paleo-liquefaction Database, Uncertainties Associated with Paleo-liquefaction Data, and Guidance for Seismic Source Characterization: Central and Eastern United States Seismic Source Characterization for Nuclear Facilities, Appendix E." Report NUREG-2115, U.S. Nuclear Regulatory Commission (NRC), Rockville, MD.

Tuttle, M.P., Dyer-Williams, K., and Barstow, N.L. (2002a). "Paleoliquefaction study of the Clarendon-Lindon fault system, western New York State." *Tectonophysics* 353: 263-286.

Tuttle, M.P., Schweig, E.S., Sims, J.D., Lafferty, R.H., Wolf, L.W. and Haynes, M.L. (2002b). "The earthquake potential of the New Madrid Seismic Zone." *Bull of the Seismological Society of America* 92(6): 2080-2089.

Tuttle, M.P., Schweig, E.S., Campbell, J., Thomas, P.M., Sims, J.D. and Lafferty, R.H. (2005). "Evidence for New Madrid earthquakes in A.D. 300 and 2350 B.C." *Seismological Research Letters* 76: 489-501.

USGS (2017). "M 9.3 scenario earthquake – Cascadia megathrust – whole CSZ characteristic M branch." *USGS National Earthquake Information Center*, available from < https://earthquake.usgs.gov/scenarios/eventpage/bssc2014cascadia_sub0_m9p34_se#executive>.

van Ballegooy, S., Malan, P., Lacrosse, V., Jacka, M.E., Cubrinovski, M., Bray, J.D., O'Rourke, T.D., Crawford, S.A. and Cowan, H. (2014). "Assessment of liquefaction-induced land damage for residential Christchurch." *Earthquake Spectra* 30(1): 31-55.

Wair, B. R., DeJong, J. T., & Shantz, T. (2012). "Guidelines for estimation of shear wave velocity profiles." Pacific Earthquake Engineering Research Center.

Wakamatsu, K. (1993). "History of soil liquefaction in Japan and assessment of liquefaction potential based on geomorphology." A Thesis in the Department of Architecture Presented in Partial Fulfillment of the Requirements for the Degree of Doctor of Engineering, Waseda University, Tokyo, Japan.

Watt, J.T., Brothers, D.A., Bennett, S.E.K., Kluesner, J.W., Roland, E., Conrad, J.E., Sliter, R.W., Dartnell, P., Goldfinger, C., Patton, J., Michalak, M.J., Sherrod, B.L., Gomberg, J., and Wells, R.E. (2017). "Toward a systematic characterization of Cascadia upper plate morphology, structure, and Quaternary deformation history: an integrated onshore-offshore approach." *GSA Abstracts* 49(6): 58.

Whistler, J.E., Atwater, B.F. and Montgomery, D.R. (2002). "Holocene liquefaction near the Seattle fault at the Issaquah Creek delta". *Eos* 83: S22B–1036.

Wirth, E.A., Frankel, A.D., Marafi, N., Vidale, J. E., and Stephenson, W. J. (2018). "Broadband Synthetic Seismograms for Magnitude 9 Earthquakes on the Cascadia Megathrust based on 3-D Simulations and Stochastic Synthetics (Part 2): Rupture Parameters and Variability." *Bulletin of the Seismological Society of America*, 108 (5A): 2370-2388.

Youd, T.L., and Noble, S.K. (1997). "Liquefaction criteria based on statistical and probabilistic analyses." In *Proc., NCEER Workshop on Evaluation of Liquefaction Resistance of Soils, NCEER Technical Rep. No: NCEER-97* 22:201-205.

Zehfuss, Z.H. (2005). "Distal records of sandy Holocene lahars from Mount Rainier, Washington". Ph.D. dissertation, University of Washington, Seattle, Washington.

Zhu, J., Baise, L.G., and Thompson, E.M. (2017). "An updated geospatial liquefaction model for global application." *Bulletin of the Seismological Society of America*, 107(3): 1365–1385.